Response to Referee #1

We would like to thank Referee #1 to review our manuscript again. Here we reply to the comments. The review comments are copied in red, and our responses are in black.

I am impressed by the seriousness the authors revision of their paper, particularly the improved meteorological analysis. There are still a few pending issues that I am listing hereafter.

Major issues:

- Topography correction. My question about the biases due to topography are still present. I feel it is important to remove any potential sampling biases due to variations in topography before comparing regional XCH4. In my original review I showed how there could be non-trivial biases over Japan (albeit using a different retrieval product).

We agree that the topography could be a cause of bias in GOSAT retrievals. However, we think that the topography effect should be minimal in our study because the GOSAT XCH_4 we uses were observed at low surface elevations. Table S1 and Figure S1 summarise the surface elevations of GOSAT XCH_4 over Northeast Asia. 95% of GOSAT data were obtained at elevation below 500 m (Table S1). Over the entire period, the highest elevation is around 1200 m and the elevations of more than 1000m are less than 0.1% in the total. The soundings in the summer 2012 and 2013 of which the periods we discussed in this study were obtained at the surface elevations below ~800m. The average elevations are 141m for 2012 and 94m for 2013. Furthermore, as shown in Figure S1, both elevation distributions for 2012 and 2013 are almost similar to the mean elevation distribution.

Table S1: Summary of Surface Elevation of GOSAT XCH_4 retrievals over Northeast Asia. All indicates the entire period of June 2009 to March 2014, for which we analysed in this study.

Period	<150 m [%]	< 500m [%]	mean elevation [m]	highest elevation [m]
All	81.6	95.0	107	1136
Aug-Sep, 2012	82.7	89.3	141	803
Aug-Sep, 2013	80.3	96.7	94	809

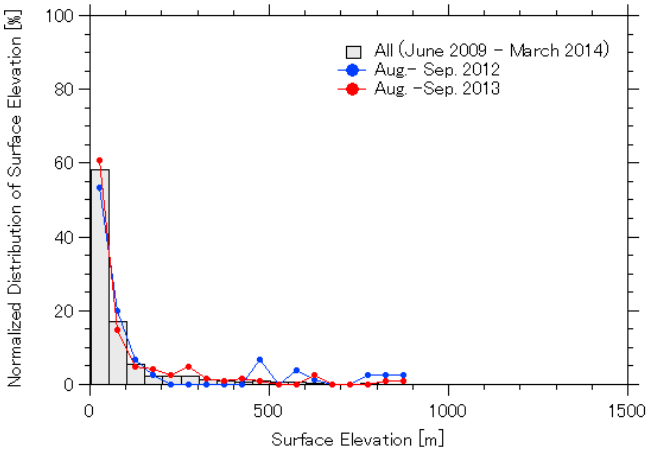

Figure S1: Normalized distribution of surface elevation of NIES GOSAT L2 XCH_4 over Northeast Asia (115E-145E, 30-40N).

Next, to test the statistical significance and possible impact of topography, we made a similar analysis with that the Referee did in the original review. Figure S2(a) shows the relationship between all the GOSAT data over Northeast Asia region of interest and the surface elevations and its linearly fitted line. The slope is -0.0128 ±0.0018 (ppb/m) and correlation coefficient is r= -0.11. The GOSAT XCH_4 time series varies temporarily with long-term trend and seasonal cycle. Next, to see how the topography impact is persistent, we first removed the long-term and the seasonal cycle from the GOSAT data, and then we applied the linear regression to the remaining GOSAT data. The long-term and seasonal components were obtained by applying the same fitting procedures that we used in this study. Figure S2(b) shows the relationship between the de-trended/de-seasoned GOSAT data and surface elevation. Same with Fig. S2(a), but a slightly weak linearity between the GOSAT data and surface elevation (slope -0.0083 ±0.00115 (ppb/m), r= -0.009) is displayed.

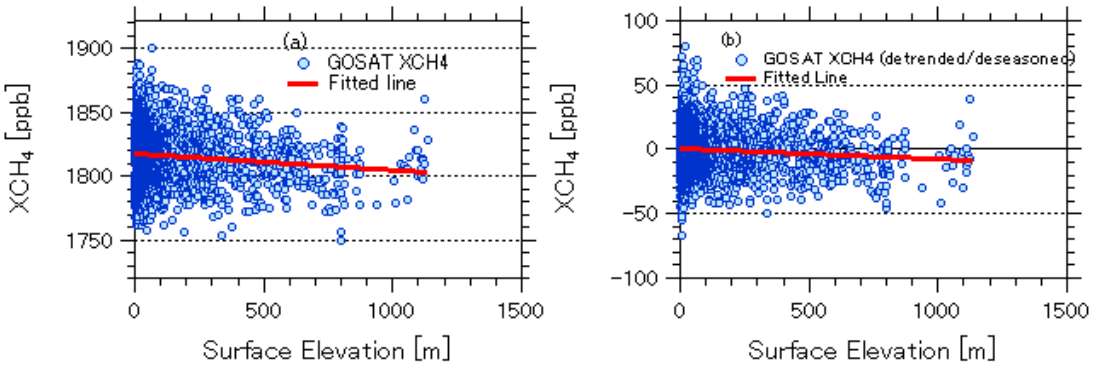

Figure S2 (a) GOSAT XCH_4 data over Northeast Asia and their linear regression against the surface elevations. (b) same with (a), but XCH_4 data are subtracted the long-term trend and season cycle.

We applied the correction of the above linear regression to the GOSAT data we used:

$XCH_4\_corr = XCH_4\_raw + 0.0083 * elevation,$ Eq. S1

where XCH_4_raw is raw GOSAT retrieval and XCH_4_corr is topograhy-corrected.

Figure S3 shows the raw GOSAT time series and topography-corrected GOSAT time series over Japan. The long-term trend and monthly means are also plotted for the both time-series. All the corrected data are shifted up slightly according to their elevations. As a result, the long-term trend lines are also shifted up slightly. Even after the topography correction is applied, the XCH_4 enhancement in summer 2013 over Japan is still outstanding and overall characteristic is unchanged.

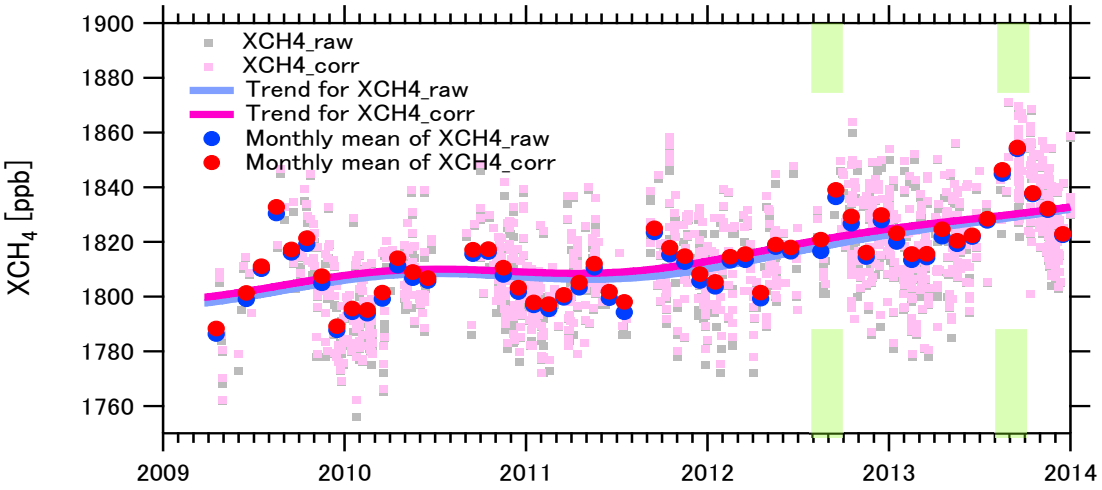

Figure S3: Comparison of raw GOSAT XCH_4 and topography-corrected GOSAT XCH_4 (by Eq S1) over Japan. The Long-term trend curves and monthly averages are also plotted for raw XCH_4 and corrected XCH_4. August-September of 2012 and 2013 are highlighted

Kort et al. (2014 GRL) applied the elevation correction to SCIAMACHY XCH_4 by a 3 order polynomial fitting curve. The elevation impact is mainly exhibited over the Rocky Mountains because of the contribution of low CH_4 air in the stratosphere. The mountainous area in our target of interest is mainly in the central Japan. In fact, few GOSAT retrievals over the

mountainous area are available in GOSAT dataset we used due to screening. As seen in Figs. S1(b) and (c), the linear regression results show that the GOSAT XCH_4 tends to be lowered with elevation. The topography should be considered as a cause of biases as well as the other possible bias factors. However, at this stage, we think the topography influence on our analysis is marginal because (1) the most retrievals were obtained in the low elevation (<500m) and (2) the topography correction derived above does not appear to be statistically significant. Therefore, in our study, any topography correction is not needed to apply to the GOSAT data we used. We have added the following sentences regarding the elevation correction in Sect. 2.1 "GOSAT XCH_4":

Kort et al. (2014) applied the elevation correction to SCIAMACHY XCH_4 over in the Southwest USA. The elevation impact is mainly exhibited over the Rocky Mountains because of low CH_4 air in the stratosphere. Surface elevation/topography could be one of potential biases in GOSAT XCH_4. However, for the GOSAT data we used, we found no statistically significant correlation with surface elevation (< r= -0.11) and also the GOSAT XCH_4 data sampled at elevation of more than 1000m is a few (~0.1% out of total). Therefore, no elevation correction was applied to the GOSAT XCH_4 in this study.

- Real vs. Noise. Figure 9 raises some other questions about the XCH4 anomaly. In particular, the model seems to agree very well in August/September 2013 with GOSAT observations over China/Korea (panel a), TCCON at Saga (panel c), and TCCON at Tsukuba (panel d). However GOSAT observations over Japan are about 20ppb higher than the model in August/September 2013. Why does the model agree with everything except for GOSAT over Japan? This also seems contrary to Fig. 5 where the authors show agreement between GOSAT and TCCON at Saga and Tsukuba. Why would the model be able to capture XCH4 at Tsukuba and Saga but not GOSAT observations over Japan?

First of all, we have to admit that we sampled the model output XCH_4 at the diagonally one-model grid shifted to the south-west direction (one model grid is $2.5^\circ \times 2.5^\circ$). Now Fig 9 has been corrected. Overall the model-observation agreement has been slightly improved, including for model and GOSAT over Japan. However, there is no tangible change in the model-observation correlations, and the statistical confidence remains same. Therefore, we think the model captures the observed variations of GOSAT XCH_4 including over Japan. To answer the referee's comment, we examined the differences between the model and GOSAT observation over Japan.

We assume that the Referee pointed out the discrepancy between model and GOSAT over Japan, especially at the end of August 2013. In the old Fig 9, the discrepancy is ~20 ppb as the Referee said, and now in the corrected Fig. 9, the discrepancy is reduced into 15 ppb. So partially the model-observation mismatch was caused by miss-sampling of model output.

Next, we investigated the GOSAT observation on August 28, 2013, and found that GOSAT targeted the Saga TCCON site on that day! GOSAT passed over Saga site, and the sounding was observed at 4:27UT (13:27 Local Time (LT)). Figure S4 show the XCH_4 observed at the Saga TCCON site and by GOSAT on August 28, 2013. Saga TCCON XCH_4 shows relatively large temporal variation with amplitude of 15 ppb. The GOSAT XCH_4 shows a good agreement with the Saga TCCON XCH_4, and it is higher than the daily mean Saga XCH_4 by 4 ppb. The daily mean TCCON XCH_4 values were compared with the modelled XCH_4 (mean over 12-15LT), after both time series were de-trended. As shown in Fig. 9, the modelled XCH_4 is lower than Saga XCH_4 by ~10 ppb on August 28, 2013. Adding the model-observation difference for Saga into the observation difference between GOSAT and Saga XCH_4, the difference between the model-GOSAT XCH_4 is expected to be ~14ppb, which is comparable to the difference seen in Fig. 9.

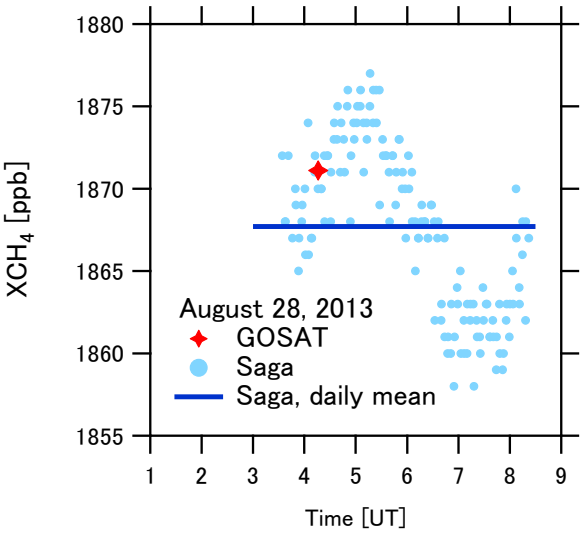

Figure S4: GOSAT XCH_4 over Japan and XCH_4 at Saga TCCON site on August 28, 2013. GOSAT XCH_4 was observed at 4:27UT (13:27 JST). JST is +9 UT. On August 28, 2013, only one GOSAT XCH_4 retrieval is available over Japan, which was observed over Saga TCCON site (the location is indicated in Figure S5)

Another issue is the availability of GOSAT XCH_4 over Japan. While TCCON sites are spatially unchanged, the number of sampling points of available GOSAT XCH_4 varies with time. Compared with Japan, more GOSAT data are usually available over China-Korea partially due to flatter surface than Japan. The discrepancy of model-GOSAT XCH_4 over Japan tends to be large when the number of available GOSAT retrievals is small. On August 28, 2013, the available GOSAT XCH_4 for Japan region is only the one over Saga. As shown in Fig. S5, the modelled XCH_4 over Japan are spatially variable. This indicates that individual GOSAT XCH_4 observations over Japan might have deviations from the "mean" XCH_4 over Japan. In despite of the limitation of sampling, collectively the GOSAT XCH_4 observations over Japan capture the enhanced XCH_4 in summer 2013 as shown in this study.

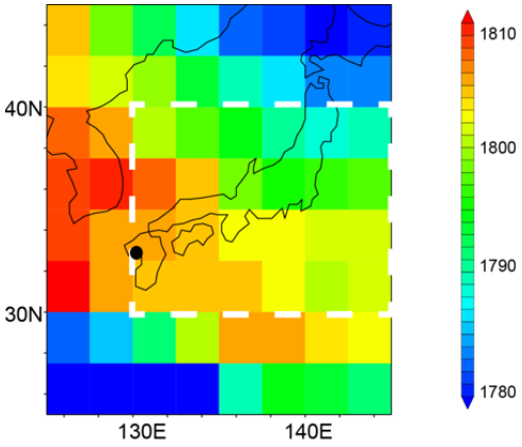

Figure S5: Modelled XCH_4 for August 28, 2013. The averaged modelled XCH_4 for 12-15 JST (3-6 UT) are plotted. The region for Japan defined in this study is enclosed in white dotted line. Saga TCCON site is indicated in black marker. It is noted that simulated XCH_4 is lower than the observed. The forward model was run with cycle-stationary surface CH_4 emissions to examine the inter-annually varying transport effect on the spatial distribution of atmospheric CH_4 and XCH_4 distributions.

The regionally averaged modelled XCH_4 over Japan is shown in Figure S6. The regional modelled XCH_4 increases during the summer of 2013. The modelled XCH_4 for GOSAT observations are almost in phase with the regional averaged modelled XCH_4, but not completely the same. Given the variance between GOSAT and TCCON, the availability of GOSAT observation, and other possible retrieval errors in GOSAT XCH_4, the modelled XCH_4 relatively capture the temporal variations of GOSAT observations over Japan.

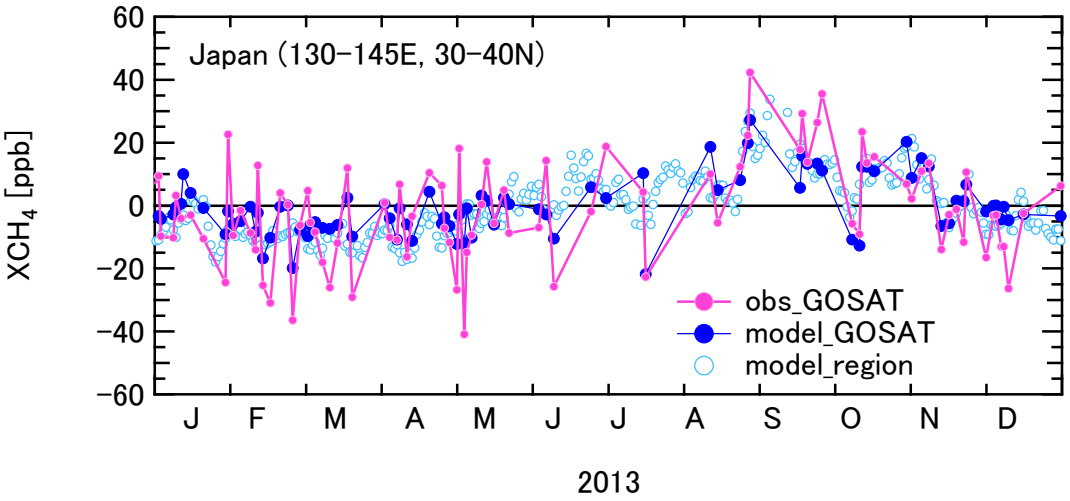

Figure S6: Model simulated XCH_4 in comparison with the observed GOSAT XCH_4. Both modelled and observed XCH_4 are daily averaged when multiple GOSAT retrievals are available. The regional averages of modelled XCH_4 over Japan are also plotted at daily time step.

Large XCH_4 anomaly in summer 2013 over Northeast Asia observed by GOSAT

M. Ishizawa[1], O. Uchino[1], I. Morino[1], M. Inoue[1*], Y. Yoshida[1], K. Mabuchi[1], T. Shirai[1], Y. Tohjima[1], S. Maksyutov[1], H. Ohyama[2], S. Kawakami[3], A. Takizawa[4] and D. Belikov[1,5,6]

[1]{National Institute for Environmental Studies, Tsukuba, Japan}

[2]{Solar-Terrestrial Environmental Laboratory, Nagoya University, Nagoya, Japan}

[3]{Japan Aerospace Exploration Agency, Tsukuba, Japan}

[4]{Japan Meteorological Agency, Tokyo, Japan}

[5]{Tomsk State University, Tomsk, Russia}

[6]{National Institute of Polar Research, Tachikawa, Japan}

[*]{now at: Akita Prefectural University, Akita, Japan}

Correspondence to: M. Ishizawa (ishizawa.misa@nies.go.jp)

Abstract

Extremely high levels of column-averaged dry-air mole fractions of atmospheric methane (XCH_4) were detected in August and September 2013 over Northeast Asia (~20 ppb above the averaged summertime XCH_4 over 2009-2012, after removing a long-term trend), as being retrieved from the Short-Wavelength InfraRed (SWIR) spectral data observed with the Thermal And Near-infrared Sensor for carbon Observation - Fourier Transform Spectrometer (TANSO-FTS) onboard Greenhouse Gases Observing Satellite (GOSAT). Similar enhancements of XCH_4 were also observed by the ground-based measurements at two Total Carbon Column Observing Network (TCCON) sites in Japan.

The analysis of surface CH_4 concentrations observed at three monitoring sites around the Japan islands suggest that the extreme increase of XCH_4 has occurred in a limited area. The model analysis was conducted to investigate this anomalously high

XCH_4 event, using an atmospheric transport model. The results indicate that the extreme increase of XCH_4 is attributed to the anomalous atmospheric pressure pattern over East Asia during the summer of 2013, which effectively transported the CH_4-rich air to Japan from the strong CH_4 source areas in East China. The two Japanese TCCON sites, ~1,000 km east-west apart each other, coincidentally located along the substantially CH_4-rich air flow from East China. This analysis demonstrates the capability of GOSAT to monitor an XCH_4 event on a synoptic scale. We anticipate that the synoptic information of XCH_4 from GOSAT data contributes to improve our understanding of regional carbon cycle and the regional flux estimation.

1 Introduction

Atmospheric methane (CH_4) is the second important anthropogenic greenhouse gas after carbon dioxide (CO_2), contributing about 20 % of the total radiative forcing from the major well-mixed greenhouse gases (Forster et al., 2007). Methane has multiple natural and anthropogenic sources in the Earth's surface while being mainly removed through reaction with hydroxyl radical (OH) in the troposphere and by photolysis in the stratosphere. The atmospheric CH_4 level has more than doubled since the onset of the industrial revolution in the 18th century (Etheridge et al., 1998). Its growth rate has been considerably variable over the past few decades (Dlugokencky et al., 2009). On a global scale, the causes of recent changes in the CH_4 growth rate remain unknown (e.g. Kirschke et al., 2013; Dlugokencky et al., 2009), and on a regional scale, significant discrepancies have been found in the emission estimates between bottom-up and top-down approaches (e.g. Miller et al., 2013). On the other hand, given the larger radiative forcing than carbon dioxide, it has been argued that reducing anthropogenic CH_4 emission might be a mitigation of possible severe impact of global warming (e.g. Hansen and Sato, 2004). Therefore, to elucidate the drivers of changes in atmospheric CH_4 concentrations and to quantify the regional source distributions are challenging tasks.

The temporal variations of observed atmospheric CH_4 are complicated due to various sources on the Earth surface, interactions between the emission sources and the atmospheric transport, and removal in the atmosphere. To improve the regional

CH_4 flux estimates on the Earth surface, it is needed to better understand the relative contribution of atmospheric transport to the observed variations of atmospheric CH_4.

In the past decades, the investigations of the spatiotemporal variability in atmospheric CH_4 concentrations and the inverse modeling estimates of surface CH_4 flux estimates had been mainly based on the ground-based measurements including aircraft and shipboard measurements (e.g. Bousquet et al., 2006; Bergamaschi et al., 2010; Miller et al., 2013). However, the current ground-based measurements of CH_4 are still sparse. In the recent years, the measurements from the satellites have been providing the large spatial and temporal coverage to help better understand the variations of atmospheric CH_4. Greenhouse gases Observing SATellite (GOSAT) was launched in January 2009,-providing column-averaged dry-air mole fractions of atmospheric CH_4 (XCH_4) that are retrieved from Short-Wavelength InfraRed (SWIR) solar spectra observed onboard Thermal And Near infrared Sensor for carbon Observation - Fourier Transform Spectrometer (TANSO-FTS) instrument (Yokota et al., 2009; Yoshida et al., 2013). The GOSAT TANSO-FTS aims at measurements of atmospheric CH_4 concentrations in three-month averages with an accuracy of better than 2 % at 100-1,000 km spatial resolution (Kuze et al., 2009). GOSAT XCH_4 is preceded by the several previous and on-going satellite projects, for example, the Infrared Atmospheric Sounding Interferometer (IASI, Crevoisier et al., 2009), and the Tropospheric Emission Spectrometer (TES, Wecht et al., 2012) and the SCanning Imaging Absorption spectroMeter for Atmospheric CHartographY (SCIAMACHY, Schneising et al., 2011). Among them, XCH_4 retrievals from SCIAMACHY instrument onboard ENVISAT launched in 2003 was pioneering, but the communication with ENVISAT was lost in April 2012. These satellite data have been used for the inversion studies of surface CH_4 emissions. Most of the satellite-based inversions are focused on the global-scale estimates (e.g., Bergamaschi et al. 2007; 2009; 2013; Fraser et al., 2013; Moteil et al, 2013; Cressot et al, 2014; Houweling et al., 2014; Alexe et al., 2015). Recently the satellite data have been applied for the flux estimation on a regional- and local-scale at a higher spatial resolution. For example, Wecht et al. (2014) compared the multiple observational constraints including GOSAT and TES to optimize methane emission in California. Turner et al. (2015) estimated North American methane emission at a resolution of up to 50 km × 50 km using GOSAT data. Kort et al. (2014) demonstrated that satellite-based observations

can quantify localized anthropogenic CH_4 emissions in the Southwest USA using the SCIAMACHY and Total Carbon Column Observing Network (TCCON) data.

Here, we report the extremely high XCH_4 event observed by GOSAT in August and September 2013 over Northeast Asia. Similar high XCH_4 event were also detected by the ground-based measurements at the two Japanese TCCON sites in Tsukuba and Saga. Given the spacing and temporal frequency (three-day recurrence) of GOSAT sampling, along with possible retrieval biases of XCH_4 retrievals, it is interesting that the GOSAT detected the synoptic-scale variation of XCH_4 that is coherent with the ground-based measurements. This GOSAT-detected XCH_4 event suggests the potential of GOSAT XCH_4 analysis in higher temporal and spatial resolution. The capability to capture synoptic-scale variations of atmospheric CH_4 leads to better regional flux estimation because the synoptic-scale variations of atmospheric CH_4 can carry the information on regional surface fluxes. On the other hand, the atmospheric CH_4 concentrations are highly changeable with the atmospheric transport as well as surface fluxes. Toward improving regional flux estimation, it is essential to observe better a synoptic-scale variation of the atmospheric CH_4 and quantify the attribution of such variations.

In this study, we analyse the extremely high XCH_4 observed by GOSAT in the summer of 2013 and investigate the attributions of such a significant increase of XCH_4. We discuss how capable GOSAT XCH_4 is to monitor synoptic-scale XCH_4 variations.

2 Observations

2.1 GOSAT XCH_4

GOSAT is a joint project of the Japanese Ministry of the Environment (MOE), the National Institute for Environmental Studies (NIES) and the Japan Aerospace Exploration Agency (JAXA) to monitor the global distribution of atmospheric CO_2 and CH_4 from space (Yokota et al., 2009). The retrieved XCH_4, as a part of NIES GOSAT Level 2 (L2) product (v02.xx), has been reported to have a mean bias of -5.9 ppb and mean standard deviation of 12.6 ppb against the XCH_4 at selected TCCON sites (Yoshida et al., 2013). In this study, we analysed NIES GOSAT L2 XCH_4

(v02.21) without any bias correction. The description of the latest updated retrieval procedures and the auxiliary information can be found at GOSAT User Interface Gateway (https://data.gosat.nies.go.jp).

We analysed GOSAT XCH_4 over two regions in Northeast Asia separately (Fig. 1). One is over northeastern China-Korea (115˚E-130˚E, 30˚N-40˚N), and the other is over Japan (130˚E-145˚E, 30˚N-40˚N). The northeastern China-Korea region covers highly populated and industrialized areas with large anthropogenic CH_4 sources in the Eurasia continent. The Japan region has small CH_4 sources, but located downwind of the continental CH_4 emissions. Time-series of XCH_4 data from June 2009 to March 2014 over the two regions with monthly means are shown in Fig. 2. It is noted that we used only the XCH_4 over land to minimize possible errors depending on sounding observation mode (Fig. 3). In fact, since a few soundings over ocean around East Asia were retrieved, removed XCH_4 data through this criterion are less than 5% of the total. A long-term trend component in each XCH_4 dataset derived through a digital filtering of two-year cutoff period (Nakazawa et al., 1997) is also plotted in Fig. 2. To focus the seasonal variations, the trend components were removed, and the detrended XCH_4 time-series are further analysed.

The GOSAT XCH_4 retrievals over Northeastern China-Korea have clear seasonality with high peaks in summer and low peaks in winter. The summertime high XCH_4 appear to be influenced by the seasonal biogenic CH_4 emissions from rice paddies and natural wetlands underneath in East China and Korea. The summer peak in 2013 was more prominent than the preceding two years, 2011 and 2012. Also, the summertime XCH_4 retrievals over Northeastern China-Korea in 2009 and 2010 were relatively high while no significantly high XCH_4 was observed over Japan. Since there is a limited number of retrieval available over Japan for the first two years of the GOSAT operation, it is difficult to discuss the XCH_4 difference over the two regions for 2009 and 2010. We thus leave this topic for a future investigation.

The seasonality of the GOSAT XCH_4 retrieval over Japan is overall similar to Northeastern China-Korea. Although the seasonal cycle varies largely year-to-year, XCH_4 retrievals of August and September in 2013 were outstandingly high. Japan is located downwind of strong anthropogenic and natural biogenic CH_4 emissions in the continent, and then the signals of the continental CH_4 emissions are lowered as the air is transported. However, it is noticeable that, in the summer of 2013, the XCH_4

retrievals over both Japan and Northeastern China-Korea regions reached the almost same high levels. This comparable XCH_4 levels in the two regions indicates there was a mechanism of fast atmospheric transport in 2013 to bring CH_4-rich air to Japan with less diffusion than the preceding years.

The number of GOSAT retrievals over Japan increased in 2013 and 2014, compared with those in the previous years. This increase is due to the change of the observation strategy to increase available GOSAT retrievals over Japan. The initial regular schedule, there were fewer soundings over lands, but most soundings were over oceans or land-ocean mixed locations. The soundings over ocean or mixed locations are difficult to be retrieved. As a result, a few retrievals remained over Japan after screening. Aiming at increasing the retrievals over Japan, the observation locations were moved inland from ocean and mixed locations as much as possible. The observation strategy change was made as a concerted decision by GOSAT Project terms among the three agencies NIES, JAXA, and MOE. This observation change was implemented on May 6, 2013.

The spatial maps of GOSAT retrievals we used in this study are shown in Fig. 3. As seen in Fig. 3a, most of the soundings were taken at lower surface elevation; more than 80% is below 100 m, 95% is below 500 m. The spatial maps of the retrievals in August and September in 2012 and 2013 are shown in Fig. 3b and Fig. 3c, respectively. Kort et al. (2014) applied the elevation correction to SCIAMACHY XCH_4 over in the Southwest USA. The elevation impact is mainly exhibited over the Rocky Mountains because of low CH_4 air in the stratosphere. Surface elevation/topography could be one of potential biases in GOSAT XCH_4. However, for the GOSAT data we used, we found no statistically significant correlation with surface elevation ($< r= -0.11$) and also the GOSAT XCH_4 data sampled at elevation of more than 1000m is a few (~0.1% out of total). Therefore, no elevation correction was applied to the GOSAT XCH_4 in this study. In Figs. 3 (b) and (c), the observation strategy change mentioned above is noticeable, the coverage of retrievals over Japan was dramatically increased in 2013, compared with 2012. As far as the China-Korea, there is no significant difference between 2012 and 2013.

2.2 TCCON XCH_4

Inside the Japan region of this study, ground-based XCH_4 measurements have been conducted at two TCCON sites, Saga (33.24˚N, 130.29˚E) and Tsukuba (36.05˚N,

140.12˚E) as shown in Fig. 1. TCCON is a worldwide network of ground-based high-resolution FTSs, which record spectra of the direct sunlight in the near-infrared, and provides accurate and precise column-averaged dry-mole fractions of atmospheric constituents including CO_2, CH_4, N_2O, HF, CO, H_2O, and HDO retrieved from these spectra absorbed by them (Wunch et al., 2011). The TCCON XCH_4 measurements have an estimated uncertainty of 7 ppb (2σ) (Wunch et al., 2010). TCCON data play a critical role in the validation of space-based measurements. The Saga TCCON site is in Kyushu Island, operated by JAXA since June, 2011. The Tsukuba TCCON site is located ~50 km north of Tokyo in the Japan main island, operated by NIES since 2009. These two Japanese TCCON sites are apart ~1,000 km longitudinally. In this study, we use the TCCON data processed by GGG 2012.

Figure 4 shows XCH_4 retrievals at Saga and Tsukuba TCCON sites during the period for 2011 to 2014. We processed the both TCCON XCH_4 time-series in the same manner with the GOSAT XCH_4 to obtain the long-term trends that are shown in blue lines in Fig. 4. It is interesting that, before the summer 2013, XCH_4 retrievals at Tsukuba overall are lower than at Saga. Since Saga is located closer to the continent than Tsukuba, Saga is considered to be influenced by the continental anthropogenic CH_4 emissions more strongly than Tsukuba. In the summer of 2013, extremely high XCH_4 retrievals both at Saga and Tsukuba were observed, reaching almost a same level. This XCH_4 enhancement observed at the ground-based TCCON sites is coincident with the high XCH_4 observed by GOSAT, and strongly supports our speculation that the CH_4 rich air was transported quickly from the continent to Japan for this period.

To focus on the seasonal and synoptic variations, we compared the detrended XCH_4 time-series from GOSAT over Japan and the two Japanese TCCON sites. Figure–5a shows that all the detrended XCH_4 data are overall in phase of seasonal cycle with seasonal amplitude of ~20 ppb. Compared with TCCON XCH_4, GOSAT XCH_4 shows large short-term variability. In 2013, both GOSAT and TCCON XCH_4 together rapidly increased in August and remained high in September. In 2012, both GOSAT XCH_4 and TCCON XCH_4 show no clear tendency in August, and all of them appear to be upward in September. On average, the XCH_4 level of GOSAT over Japan in August and September 2013 is higher by ~15 ppb than 2012. The XCH_4 levels of

both TCCON sites in 2013 are higher by ~20 ppb than 2012. These enhancements of XCH_4 are comparable to their seasonal amplitude.

To examine further how the synoptic variability of GOSAT is correlated with TCCON, we removed the mean seasonal cycles from the detrended XCH_4 time-series and took the monthly means (Fig. 5b). Except the months when the retrievals are available for less than two days, the correlation coefficients (r) of the monthly means between GOSAT and TCCON at Saga, and between GOSAT and TCCON at Tsukuba, are 0.81 and 0.61, respectively. These correlation coefficient values exceed the 95% significance level. Despite the large short-term variability, the synoptic variability of GOSAT over Japan is overall correlated with the TCCON XCH_4 at two Japanese sites. The enhancement of XCH_4 in the summer of 2013 is consistent among GOSAT and TCCON. If the period is limited to May–December 2013, when the number of GOSAT XCH_4 retrievals was increased due to the observation strategy change mentioned earlier, the correlation coefficients (r) between GOSAT and TCCON are improved to be 0.91 with Saga and 0.96 with Tsukuba. This implies that the increase in the observations over Japan improves the capability of GOSAT to detect synoptic variability in XCH_4.

2.3 Ground-based surface CH_4 concentrations

In order to see the relationship between the surface CH_4 concentration and the enhancement of GOSAT XCH_4 over Japan, we analyzed the surface CH_4 concentrations observed at three ground-based monitoring stations in Japan, Cape Ochi-ishi (COI, 43.16˚N, 145.49˚E), Ryori (RYO, 39.03˚N, 141.82˚E), and Yonagunijima (YON, 24.47˚N, 123.02˚E). These site locations are shown in Fig. 1. At all the stations, continuous measurements of atmospheric CH_4 are conducted. Cape Ochi-ishi (COI) is a station operated by NIES, which is located at the east tip of Hokkaido island (Tohjima et al., 2002). Ryori (RYO) is located inside the Japan region defined in this study, where the monitoring of surface greenhouse gas concentrations has been conducted by the Japan Meteorological Agency (JMA) as a part of the Global Atmospheric Watch (GAW) program of the World Meteorological Observation (WMO). RYO is on the west coast of the Japan main island, about 300 km north of Tsukuba and far away from direct influences of residential and industrial

pollutants. Yonagunijima (YON) is also one of JMA-operated GAW stations, which is located far south of the Japan main island and east of ~110 km of Taiwan. The details on RYO and YON are provided on the web page of WMO GAW World Data Centre for Greenhouse Gases (WDCGG) (http://ds.data.jma.go.jp/gmd/wdcgg/introduction.html).

The time-series of surface CH_4 concentrations at the three ground-based stations are shown in Fig. 6, with their monthly means and long-term trends. Here we analyzed the afternoon mean CH_4 (averaged hourly CH_4 over 12:00 - 15:00 local time) from the respective data sets, assuming that the afternoon values are large-scale representative. The observed CH_4 concentrations at all the sites show similar seasonal cycles in timing. Seasonally the CH_4 values are low in July and August, and high in winter to spring. In the winter, the westerly wind prevails and transports the CH_4-rich air from the continent (mainly anthropogenic CH_4 emitted in East China) to Japan, causing the rise of CH_4 concentrations. In the summer, the southeasterly wind is dominant, bringing clean air to Japan from the Pacific Ocean, where is no major CH_4 source, so that the surface CH_4 concentrations become low.

In the summer of 2013, unseasonably high CH_4 concentrations were observed at RYO with a sharp increase in the middle of August. The CH_4 concentrations at COI started increasing earlier from its summer minimum than the previous year, 2012. At YON, no significant CH_4 enhancement was seen in 2013 compared with the previous years. Since no similar CH_4 change to RYO and COI was observed at YON, the farthest southwestern island of Japan, this significant CH_4 enhancement event appears to be spatially limited in the area around Japan main island and Hokkaido island. To further examine the summer increase of surface CH_4 concentrations, we compared the detrended CH_4 at RYO and COI for the two years of 2012 and 2013 (Fig. 7). The timing and amplitude of seasonal cycles at RYO and COI overall agree well with each other, except for the summer of 2013. In August and September of 2013, the temporal variations of CH_4 at RYO and COI are different from those in the previous year 2012 when the CH_4 concentrations were low over the summertime and started rising at the end of September. In August 2013, the abrupt CH_4 increase by ~100 ppb was observed at RYO, followed by COI with ~1 week delay. In September, the CH_4 at both sites lowered but stayed in the higher level than 2012. Given that the fact the major CH_4 sources in East China, the sudden large increase of CH_4 in August 2013 is

probably caused by unseasonal transport of CH_4-rich air from the continent to Japan though normally in August the wind with CH_4-low air from the Pacific Ocean is prevailing over Japan.

3 Model analysis

The observational data analysis suggested that the atmospheric transport would be a key factor of the extreme enhancement event of XCH_4 and surface CH_4 concentrations in the summer of 2013 over Japan. To investigate how the inter-annually varying atmospheric transport plays the role in the enhancement of XCH_4 and surface CH_4, we conducted a forward model simulation using the global atmospheric transport model of National Institute for Environmental Studies (NIES-TM) version 8.1i.

The NIES-TM has a horizontal resolution of 2.5˚×2.5˚ with 32 vertical layers (Belikov et al., 2013). The global wind fields used in this study were obtained from the JMA Climate Data Assimilation System (JCDAS) (Onogi et al., 2007). The planetary boundary layer height data are obtained from the European Centre for Medium-Range Weather Forecasts (ECMWF) Interim Reanalysis dataset (Dee et al., 2011). In order to examine the impact of time-varying atmospheric transport on the seasonal cycles of atmospheric CH_4 and XCH_4 fields, the CH_4 emissions averaged over 2009-2010 were repeatedly used during the entire model simulation period for 2009-2013. The CH_4 emissions comprise anthropogenic fluxes and natural fluxes. The anthropogenic fluxes are from the Emissions Database for Global Atmospheric Research (EDGAR) inventory, v4.2 FT2010 (http://edgar.jrc.ec.europa.eu/). The natural CH_4 fluxes are biomass burning from Global Fire Emissions Database (GFED) v3.1 (van der Werf et al., 2010), wetland, rice paddy emissions and soil sinks from the Vegetation Integrative Simulator for Trace gases (VISIT) (Ito and Inatomi, 2012), and termites (Fung et al., 1991). Except the termites CH_4 emission, all the natural fluxes are seasonal. We used the modeled methane loss and climatological OH fields provided for a model inter-comparison project "TransCom-CH_4" (Patra et al., 2011).

Figure 8 shows the simulated surface CH_4 concentration and XCH_4 fields for August and September in 2012 and 2013. As a common feature, the high levels of XCH_4 and surface CH_4 are found over East China, reflecting the spatial distribution of

the strong anthropogenic emissions around Beijing and Shanghai and biogenic CH_4 sources from rice cultivation in the southeastern China.

Different patterns are found in the XCH_4 and surface CH_4 fields between 2012 and 2013. In August 2012, both levels of XCH_4 and surface CH_4 over Japan are as low as those over the Pacific oceans. In August 2013, higher concentrations of surface CH_4 extended from the northeastern China and the Korean peninsula to the Japan islands. The surface CH_4 concentration level in 2013 over Japan is increased by 40-60 ppb from the level in 2012. The XCH_4 values over Japan are also enhanced by ~20 ppb while the XCH_4 values over the southeastern China are lowered compared to the 2012 level. The lower concentrations in August 2013 over the southeastern China than 2012 indicate that the northward wind along the coast was so fast that CH_4 was not much accumulated over the CH_4 source area in the southeastern China, but transported away to the north. As a result, the areas of the highest levels of CH_4 and XCH_4 shifted to the northeast, from the southeast China. In September 2013, XCH_4 level over the southeastern China is higher than August, but still lower than the level of September 2012. Also the XCH_4 over Japan remains higher level than that of 2012. The surface CH_4 concentration pattern in September 2013 is almost similar to the one in 2012, but slightly higher values are found over Japan.

Figure 9 shows the time-series of modeled XCH_4 for GOSAT and TCCON, compared with the observations. For GOSAT, the modeled XCH_4 co-located with the GOSAT observations are sampled and averaged for comparison. The modeled XCH_4 produce the enhancement in summer 2013, in phase with the observations (Fig. 9). Overall the temporal variations of modeled XCH_4 are correlated with the observations ($r = 0.50 \sim 0.72$). These correlation coefficient values exceeded the 95% significance level. The seasonal cycles of modeled XCH_4 for GOSAT and TCCON are in good agreement with the observations, while the modeled GOSAT XCH_4 show less short-term variability than the observations. The modeled surface CH_4 concentrations for the three Japanese sites, COI, RYO, and YON, are shown in Fig. 10. Though the modeled seasonal amplitude is slightly smaller than the observed, the modeled CH_4 overall capture the observed synoptic variations, as well as the abrupt increase in August 2013 at COI and RYO. The model was run with cyclo-stationary surface CH_4 fluxes, which are seasonally varying but not inter-annually. Inside the model, only the transport field is varying inter-annually. The model-observation comparison thus

provides supporting evidence that anomalous wind field in 2013 plays a key role in the large XCH_4 event in 2013.

4 Discussions

4.1 Characteristics of Atmospheric Circulation in the summer of 2013

Forward modeling gives us insights into the contribution of atmospheric transport on the enhancement of XCH_4 and surface CH_4 concentration in the summer of 2013 over Japan. Here we examine the 2013 summertime atmospheric transport over the northeastern Asia.

Japan's summer climate is governed by the Pacific High (a lower-level high-pressure system) and the Tibetan High (an upper-level high-pressure system). These pressure systems were reported to have been enhanced during July and August 2013 (Tokyo Climate Center News No.34 Autumn 2013, available at http://ds.data.jma.go.jp/tcc/tcc/news). The Pacific High continued to expand westward and largely developed over the western part of Japanese islands including Okinawa. The Tibetan High expanded to the Japan main island in line with the northward meandering of upper-level westerly winds (the subtropical jet stream). The enhanced atmospheric transport from East China to Japan was probably attributed to those anomalously developed high-pressure systems.

To see how the 2013 summertime atmospheric transport differs from the mean transport pattern, Fig. 11 shows the wind fields at the surface and at 850 hPa pressure level, from the JCDAS wind fields of August and September in 2013 over East Asia, compared with those of the mean wind fields for the five years of 2009-2013.

At the surface level (Fig. 11a), the mean wind field clearly shows that, in August the southeasterly wind from the Pacific Ocean prevails due to the development of the Pacific High. In September the wind from the continent to Japan start blowing as the Pacific High is retiring. In August 2013, as the Pacific High expanded westward, the air moved northward along the coast of China, turned around the Korean Peninsula, and flowed to Japan. This wind pattern suggests that the CH_4-rich air was transported from East China to Japan in 2013, while the clean air is normally transported from the Pacific Ocean. In September 2013, over the Pacific

Ocean, south of the Japan main island, easterly wind was still stronger than the normal, but the wind pattern over Japan was almost back to the normal, which can be characterized as a weak convergence of westerly wind from the continent and easterly wind from the Pacific Ocean. This nearly normal wind pattern over northern Japan would lower the CH_4 concentrations at the surface level as observed at RYO and COI.

At the 850 hPa level (Fig. 11b), it is notable that, in August 2013 the air moved over the East China along the coast and turned around the Korean peninsula sharply to the Japan islands. The anomalous westerly winds were stronger in the upper levels than near the surface. Given the major CH_4 source distributions in East Asia, the strong northward air flow along the coast could reduce local CH_4 accumulation, but transport the CH_4-rich air effectively to the north and then to Japan as turning around the Korean peninsula. In September 2013, the wind speed over Japan was much lower than August, but wind still blows westerly from the continent to Japan. This slower westerly air flow could maintain the higher level of XCH_4 over Japan during the September of 2013.

The wind patterns we examined above shows us how the atmospheric transport field in 2013 differed from a climatological field on a regional-scale. In order to narrow down the origins and the upstream patterns of the air masses to the Japanese TCCON sites, we conducted back trajectory analysis using the Stochastic Time-Inverted Lagrangian Transport (STILT) model (Lin et al., 2003), driven by Global Data Assimilation System (GDAS) meteorology ($1^\circ \times 1^\circ$). To obtain the monthly mean features of the upstream, we released 100 particles from the height of 1500 m (approximately ~850 hPa) at Saga and Tsukuba, at every 12:00 noon local time (= 3 UT) and traveled backward for 10-days. Every 30 minutes, the number of particles was counted by a $1^\circ \times 1^\circ$ air column and the total number of particles over the 10 day duration was divided by the maximum number per column. Thus, we obtained a normalized daily upstream pattern and averaged them over a month. Figure 12 shows the monthly normalized trajectories for August and September in 2012 and 2013. There are distinct differences in the upstream patterns between 2012 and 2013. The patterns of the summer of 2012 are almost like climatological; in August, the wind flows dominantly from the Pacific to the Japan, in September the dominant wind direction is in transition; from southeasterly wind (from the Pacific) to northwesterly wind (from the continent). On the other hand, in August 2013 the air

masses reached the Japanese TCCON sites from the west, after traveling over the coastal side of East China. In September 2013, the westerly wind from the continent is still dominant, especially for Saga. This backtrajectory result supports that the anomalous wind field in the summer of 2013 brought the CH_4-rich air from China to Japan, resulting in the high XCH_4 observed at the two Japanese TCCON sites and also by GOSAT over Japan.

4.2 Other possible factors

Although we suggest that the atmospheric transport field probably attributes to the enhancement of XCH_4 and CH_4 concentration observed in the summer of 2013, we cannot entirely rule out other possible factors. Here we discuss two factors. One is the surface emission changes. Though the temporal variations in XCH_4 do not necessarily correlate with the surface emissions (e.g., Bloom et al., 2010), the surface emission change is potential to impact on the change in XCH_4. The second is the contribution of stratospheric methane.

The CH_4 emissions from rice cultivations and wetland in Southern China might be enhanced under the hot summer condition in 2013. East Asia around China experienced a hotter summer monsoon season (June-September) by more than 1 ˚C than the season normal (Tokyo Climate Center News No.34 Autumn 2013), while less than 60 % of the normal precipitation in eastern China was reported. A hot weather condition increases the CH_4 emissions through the enhancement of photosynthesis and methanogenic activity in inundated grounds such as wetlands and rice paddies; while a dry condition reduces the CH_4 emissions from wetlands as the water table levels in the ground become low. Thus, the hot and dry weather conditions have opposite effects on the CH_4 emissions from wetlands. The time delay in the correlation between CH_4 emissions and climate anomalies should be considered as the groundwater plays an important role in wetland CH_4 emissions. Furthermore, since rice cultivation is human-managed, multiple controlling factors on CH_4 emissions from rice paddies should be considered. A further investigation of wetland and rice CH_4 emission changes responding to the climate anomaly in East Asia is needed.

Another possibility is the contribution of stratospheric methane. Saad et al. (2014) presented the analysis that the stratospheric methane causes short-term

fractionations in total column averaged CH_4 observed at several TCCON sites. The contribution of stratospheric methane to the anomaly in summer 2013 is supposed to be minor or less influential. Firstly the surface CH_4 concentrations at COI and RYO increased in August 2013 when the XCH_4 anomaly occurred, suggesting the major contributor on the anomaly is in the troposphere. Secondly, the order of the stratospheric methane fractionation is smaller than ~3 ppb, which would not be enough to produce the anomaly of an order of ~20 ppb.

5 Conclusion

In this study, we have examined the extremely high XCH_4 event over Northeast Asia observed by GOSAT in August and September, 2013. Similar XCH_4 enhancements in amplitude and timing were observed at the two Japanese TCCON sites, Tsukuba and Saga. Furthermore, during the same period, the ground-based atmospheric CH_4 monitoring sites of Ryori and Ochi-ishi located in the northern part of Japan observed the higher levels of surface CH_4. In particular, surface CH_4 concentrations at Ryori showed the rapid increase in the middle of August 2013.

Our model analysis indicates that the significant enhancement of XCH_4 and surface CH_4 are mainly attributed to the anomalous atmospheric pressure patterns of Pacific High and Tibetan High over East Asia during the summer of 2013. The CH_4-rich air was effectively transported to Japan from the major CH_4 source area in East China. The model analysis also indicates that the XCH_4 enhancement occurred in a limited area of the northeastern China to the Japan main island. The two Japanese TCCON sites, ~1,000 km apart from each other, happened to be located along the anomalously CH_4-rich air flow from the Eurasian continent and coincidentally observed the extreme increase of XCH_4. The GOSAT with three-day recurrence successfully observed the high XCH_4 event. This data analysis study demonstrates the capability of GOSAT to monitor the synoptic-scale XCH_4 event in the association with the high-pressure system anomalies. The GOSAT capability to detect synoptic variations could be helpful to quantify the relative contribution of atmospheric transport, leading to better estimation of regional CH_4 fluxes.

Acknowledgements

Surface CH_4 data observed at Ryori and Yonagunijima are got from the WDCGG (http://ds.data.jma.go.jp/gmd/wdcgg/). TCCON data were obtained from the TCCON Data Archive, operated by the California Institute of Technology from the website at tccon.ipac.caltech.edu. The authors wish to thank two anonymous reviewers for their helpful comments to improve the manuscript.

References

Alexe, M., Bergamaschi, P., Segers, A., Detmers, R., Butz, A., Hasekamp, O., Guerlet, S., Parker, R., Boesch, H., Frankenberg, C., Scheepmaker, R. A., Dlugokencky, E., Sweeney, C., Wofsy, S. C., and Kort, E. A.: Inverse modelling of CH_4 emissions for 2010 – 2011 using different satellite retrieval products from GOSAT and SCIAMACHY, Atmos. Chem. Phys., 15, 113-133, 10.5194/acp-15-113-2015, 2015.

Belikov, D. A., Maksyutov, S., Sherlock, V., Aoki, S., Deutscher, N. M., Dohe, S., Griffith, D., Kyro, E., Morino, I., Nakazawa, T., Notholt, J., Rettinger, M., Schneider, M., Sussmann, R., Toon, G. C., Wennberg, P. O., and Wunch, D.: Simulations of column-averaged CO_2 and CH_4 using the NIES TM with a hybrid sigma-isentropic (σ-θ) vertical coordinate, Atmos. Chem. Phys., 13, 1713-1732, 10.5194/acp-13-1713-2013, 2013.

Bergamaschi, P., Frankenberg, C., Meirink, J. F., Krol, M., Dentener, F., Wagner, T., Platt, U., Kaplan, J. O., Körner, S., Heimann, M., Dlugokencky, E. J., and Goede, A.: Satellite chartography of atmospheric methane from SCIAMACHY on board ENVISAT: 2. Evaluation based on inverse model simulations, J. Geophys. Res., 112, 10.1029/2006JD007268, 2007.

Bergamaschi, P., Frankenberg, C., Meirink, J. F., Krol, M., Villani, M. G., Houweling, S., Dentener, F., Dlugokencky, E. J., Miller, J. B., Gatti, L. V., Engel, A., and Levin, I.: Inverse modeling of global and regional CH_4 emissions using SCIAMACHY satellite retrievals, J. Geophys. Res., 114, 10.1029/2009jd012287, 2009.

Bergamaschi, P., Krol, M., Meirink, J. F., Dentener, F., Segers, A., van Aardenne, J., Monni, S., Vermeulen, A. T., Schmidt, M., Ramonet, M., Yver, C., Meinhardt, F., Nisbet, E. G., Fisher, R. E., O'Doherty, S., and Dlugokencky, E. J.: Inverse modeling of European CH_4 emissions 2001–2006, J. Geophys. Res., 115, D22309, 10.1029/2010JD014180, 2010.

Bergamaschi, P., Houweling, S., Segers, A., Krol, M., Frankenberg, C., Scheepmaker, R. A., Dlugokencky, E., Wofsy, S. C., Kort, E. A., Sweeney, C., Schuck, T., Brenninkmeijer, C., Chen, H., Beck, V., and Gerbig, C.: Atmospheric CH_4 in the first decade of the 21st century: Inverse modeling analysis using SCIAMACHY satellite retrievals and NOAA surface measurements, J. Geophys. Res., 118, 7350-7369, 10.1002/jgrd.50480, 2013.

Bloom, A. A., Palmer, P. I., Fraser, A., Reay, D. S., and Frankenberg, C.: Large-Scale Controls of Methanogenesis Inferred from Methane and Gravity Spaceborne Data, Science, 327, 322-325, 10.1126/science.1175176, 2010.

Bousquet, P., Ciais, P., Miller, J. B., Dlugokencky, E. J., Hauglustaine, D. A., Prigent, C., Van der Werf, G. R., Peylin, P., Brunke, E. G., Carouge, C., Langenfelds, R. L., Lathiere, J., Papa, F., Ramonet, M., Schmidt, M., Steele, L. P., Tyler, S. C., and White, J.: Contribution of anthropogenic and natural sources to atmospheric methane variability, Nature, 443, 439-443, 10.1038/nature05132, 2006.

Cressot, C., Chevallier, F., Bousquet, P., Crevoisier, C., Dlugokencky, E. J., Fortems-Cheiney, A., Frankenberg, C., Parker, R., Pison, I., Scheepmaker, R. A., Montzka, S. A., Krummel, P. B., Steele, L. P., and Langenfelds, R. L.: On the consistency between global and regional methane emissions inferred from SCIAMACHY, TANSO-FTS,

IASI and surface measurements, Atmos. Chem. Phys., 14, 577-592, 10.5194/acp-14-577-2014, 2014.

Crevoisier, C., Nobileau, D., Fiore, A. M., Armante, R., Chédin, A., and Scott, N. A.: Tropospheric methane in the tropics – first year from IASI hyperspectral infrared observations, Atmos. Chem. Phys., 9, 6337-6350, 10.5194/acp-9-6337-2009, 2009.

Dee, D. P., Uppala, S. M., Simmons, A. J., Berrisford, P., Poli, P., Kobayashi, S., Andrae, U., Balmaseda, M. A., Balsamo, G., Bauer, P., Bechtold, P., Beljaars, A. C. M., van de Berg, L., Bidlot, J., Bormann, N., Delsol, C., Dragani, R., Fuentes, M., Geer, A. J., Haimberger, L., Healy, S. B., Hersbach, H., Hólm, E. V., Isaksen, L., Kållberg, P., Köhler, M., Matricardi, M., McNally, A. P., Monge-Sanz, B. M., Morcrette, J. J., Park, B. K., Peubey, C., de Rosnay, P., Tavolato, C., Thépaut, J. N., and Vitart, F.: The ERA-Interim reanalysis: configuration and performance of the data assimilation system, Q. J. R. Meteorolog. Soc., 137, 553-597, 10.1002/qj.828, 2011.

Dlugokencky, E. J., Bruhwiler, L., White, J. W. C., Emmons, L. K., Novelli, P. C., Montzka, S. A., Masarie, K. A., Lang, P. M., Crotwell, A. M., Miller, J. B., and Gatti, L. V.: Observational constraints on recent increases in the atmospheric CH_4 burden, Geophys. Res. Lett., 36, L18803, 10.1029/2009GL039780, 2009.

Etheridge, D. M., Steele, L. P., Francey, R. J., and Langenfelds, R. L.: Atmospheric methane between 1000 A.D. and present: Evidence of anthropogenic emissions and climatic variability, J. Geophys. Res., 103, 15979-15993, 10.1029/98JD00923, 1998.

Forster, P., Ramaswamy, V., Artaxo, P., Berntsen, T., Betts, R., Fahey, D. W., Haywood, J., Lean, J., Lowe, D. C., Myhre, G., Nganga, J., Prinn, R., Raga, G., Schulz, M., and Van Dorland, R.: Changes in atmospheric constituents and in radiative forcing, in: Climate Change 2007: The Physical Science Basis. Contribution of Working Group I to the Fourth Assessment Report of the Intergovernmental Panel on Climate Change, edited by: Solomon, S., Qin, D., Manning, M., Chen, Z., Marquis, Averyt, K. B., Tignor, M., and Miller, H. L., Cambridge University Press, Cambridge, United Kingdom and New York, NY, USA, 129-234, 2007.

Fraser, A., Palmer, P. I., Feng, L., Boesch, H., Cogan, A., Parker, R., Dlugokencky, E. J., Fraser, P. J., Krummel, P. B., Langenfelds, R. L., O'Doherty, S., Prinn, R. G., Steele, L. P., van der Schoot, M., and Weiss, R. F.: Estimating regional methane surface fluxes: the relative importance of surface and GOSAT mole fraction measurements, Atmos. Chem. Phys., 13, 5697-5713, 10.5194/acp-13-5697-2013, 2013.

Fung, I., John, J., Lerner, J., Matthews, E., Prather, M., Steele, L. P., and Fraser, P. J.: Three-dimensional model synthesis of the global methane cycle, J. Geophys. Res., 96, 13033-13065, 10.1029/91JD01247, 1991.

Hansen, J., and Sato, M.: Greenhouse gas growth rates, Proc. Natl. Acad. Sci. U.S.A., 101, 16109-16114, 10.1073/pnas.0406982101, 2004.

Ito, A., and Inatomi, M.: Use of a process-based model for assessing the methane budgets of global terrestrial ecosystems and evaluation of uncertainty, Biogeosciences, 9, 759-773, 10.5194/bg-9-759-2012, 2012.

Houweling, S., Krol, M., Bergamaschi, P., Frankenberg, C., Dlugokencky, E. J., Morino, I., Notholt, J., Sherlock, V., Wunch, D., Beck, V., Gerbig, C., Chen, H., Kort, E. A., Röckmann, T., and Aben, I.: A multi-year methane inversion using

SCIAMACHY, accounting for systematic errors using TCCON measurements, Atmos. Chem. Phys., 14, 3991-4012, 10.5194/acp-14-3991-2014, 2014.

Kirschke, S., Bousquet, P., Ciais, P., Saunois, M., Canadell, J. G., Dlugokencky, E. J., Bergamaschi, P., Bergmann, D., Blake, D. R., Bruhwiler, L., Cameron-Smith, P., Castaldi, S., Chevallier, F., Feng, L., Fraser, A., Heimann, M., Hodson, E. L., Houweling, S., Josse, B., Fraser, P. J., Krummel, P. B., Lamarque, J.-F., Langenfelds, R. L., Le Quéré, C., Naik, V., O'Doherty, S., Palmer, P. I., Pison, I., Plummer, D., Poulter, B., Prinn, R. G., Rigby, M., Ringeval, B., Santini, M., Schmidt, M., Shindell, D. T., Simpson, I. J., Spahni, R., Steele, L. P., Strode, S. A., Sudo, K., Szopa, S., van der Werf, G. R., Voulgarakis, A., van Weele, M., Weiss, R. F., Williams, J. E., and Zeng, G.: Three decades of global methane sources and sinks, Nat. Geosci., 6, 813-823, 10.1038/ngeo1955, 2013.

Kort, E. A., Frankenberg, C., Costigan, K. R., Lindenmaier, R., Dubey, M. K., and Wunch, D.: Four corners: The largest US methane anomaly viewed from space, Geophys. Res. Lett., 41, 2014GL061503, 10.1002/2014GL061503, 2014.

Kuze, A., Suto, H., Nakajima, M., and Hamazaki, T.: Thermal and near infrared sensor for carbon observation Fourier-transform spectrometer on the Greenhouse Gases Observing Satellite for greenhouse gases monitoring, Appl. Opt., 48, 6716-6733, 10.1364/AO.48.006716, 2009.

Lin, J. C., Gerbig, C., Wofsy, S. C., Andrews, A. E., Daube, B. C., Davis, K. J., and Grainger, C. A.: A near-field tool for simulating the upstream influence of atmospheric observations: The Stochastic Time-Inverted Lagrangian Transport (STILT) model, J. Geophys. Res.-Atmos., 108, Doi 10.1029/2002jd003161, 2003.

Miller, S. M., Wofsy, S. C., Michalak, A. M., Kort, E. A., Andrews, A. E., Biraud, S. C., Dlugokencky, E. J., Eluszkiewicz, J., Fischer, M. L., Janssens-Maenhout, G., Miller, B. R., Miller, J. B., Montzka, S. A., Nehrkorn, T., and Sweeney, C.: Anthropogenic emissions of methane in the United States, Proc. Natl. Acad. Sci. U.S.A., 110, 20018-20022, 10.1073/pnas.1314392110, 2013.

Monteil, G., Houweling, S., Butz, A., Guerlet, S., Schepers, D., Hasekamp, O., Frankenberg, C., Scheepmaker, R., Aben, I., and Röckmann, T.: Comparison of CH4 inversions based on 15 months of GOSAT and SCIAMACHY observations, J. Geophys. Res., 118, 11,807-811,823, 10.1002/2013JD019760, 2013.

Nakazawa, T., Ishizawa, M., Higuchi, K., and Trivett, N. B. A.: Two curve fitting methods applied to CO_2 flask data, Environmtrics, 8, 197-218, 1997.

Onogi, K., Tsutsui, J., Koide, H., Sakamoto, M., Kobayashi, S., Hatsushika, H., Matsumoto, T., Yamazaki, N., Kamahori, H., Takahashi, K., Kadokura, S., Wada, K., Kato, K., Oyama, R., Ose, T., Mannoji, N., and Taira, R.: The JRA-25 Reanalysis, J. Meteor. Soc. Japan, 85, 369-432, 10.2151/jmsj.85.369, 2007.

Patra, P. K., Houweling, S., Krol, M., Bousquet, P., Belikov, D., Bergmann, D., Bian, H., Cameron-Smith, P., Chipperfield, M. P., Corbin, K., Fortems-Cheiney, A., Fraser, A., Gloor, E., Hess, P., Ito, A., Kawa, S. R., Law, R. M., Loh, Z., Maksyutov, S., Meng, L., Palmer, P. I., Prinn, R. G., Rigby, M., Saito, R., and Wilson, C.: TransCom model simulations of CH_4 and related species: linking transport, surface flux and chemical loss with CH_4 variability in the troposphere and lower stratosphere, Atmos. Chem. Phys., 11, 12813-12837, 10.5194/acp-11-12813-2011, 2011.

Saad, K. M., Wunch, D., Toon, G. C., Bernath, P., Boone, C., Connor, B., Deutscher, N. M., Griffith, D. W. T., Kivi, R., Notholt, J., Roehl, C., Schneider, M., Sherlock, V., and Wennberg, P. O.: Derivation of tropospheric methane from TCCON CH_4 and HF total column observations, Atmos. Meas. Tech., 7, 2907-2918, 10.5194/amt-7-2907-2014, 2014.

Schneising, O., Buchwitz, M., Reuter, M., Heymann, J., Bovensmann, H., and Burrows, J. P.: Long-term analysis of carbon dioxide and methane column-averaged mole fractions retrieved from SCIAMACHY, Atmos. Chem. Phys., 11, 2863-2880, 10.5194/acp-11-2863-2011, 2011.

Tanaka, T., Miyamoto, Y., Morino, I., Machida, T., Nagahama, T., Sawa, Y., Matsueda, H., Wunch, D., Kawakami, S., and Uchino, O.: Aircraft measurements of carbon dioxide and methane for the calibration of ground-based high-resolution Fourier Transform Spectrometers and a comparison to GOSAT data measured over Tsukuba and Moshiri, Atmos. Meas. Tech., 5, 2003-2012, 10.5194/amt-5-2003-2012, 2012.

Tohjima, Y., Machida, T., Utiyama, M., Katsumoto, M., Fujinuma, Y., and Maksyutov, S.: Analysis and presentation of in situ atmospheric methane measurements from Cape Ochi-ishi and Hateruma Island, J. Geophys. Res., 107, ACH 8-1-ACH 8-11, 10.1029/2001JD001003, 2002.

Turner, A. J., Jacob, D. J., Wecht, K. J., Maasakkers, J. D., Lundgren, E., Andrews, A. E., Biraud, S. C., Boesch, H., Bowman, K. W., Deutscher, N. M., Dubey, M. K., Griffith, D. W. T., Hase, F., Kuze, A., Notholt, J., Ohyama, H., Parker, R., Payne, V. H., Sussmann, R., Sweeney, C., Velazco, V. A., Warneke, T., Wennberg, P. O., and Wunch, D.: Estimating global and North American methane emissions with high spatial resolution using GOSAT satellite data, Atmos. Chem. Phys., 15, 7049-7069, 10.5194/acp-15-7049-2015, 2015.

van der Werf, G. R., Randerson, J. T., Giglio, L., Collatz, G. J., Mu, M., Kasibhatla, P. S., Morton, D. C., DeFries, R. S., Jin, Y., and van Leeuwen, T. T.: Global fire emissions and the contribution of deforestation, savanna, forest, agricultural, and peat fires (1997–2009), Atmos. Chem. Phys., 10, 11707-11735, 10.5194/acp-10-11707-2010, 2010.

Wecht, K. J., Jacob, D. J., Wofsy, S. C., Kort, E. A., Worden, J. R., Kulawik, S. S., Henze, D. K., Kopacz, M., and Payne, V. H.: Validation of TES methane with HIPPO aircraft observations: Implications for inverse modeling of methane sources, Atmos. Chem. Phys., 12, 1823-1832, 10.5194/acp-12-1823-2012, 2012.

Wecht, K. J., Jacob, D. J., Frankenberg, C., Jiang, Z., and Blake, D. R.: Mapping of North American methane emissions with high spatial resolution by inversion of SCIAMACHY satellite data, J. Geophys. Res., 119, 7741-7756, 10.1002/2014JD021551, 2014.

Wunch, D., Toon, G. C., Wennberg, P. O., Wofsy, S. C., Stephens, B. B., Fischer, M. L., Uchino, O., Abshire, J. B., Bernath, P., Biraud, S. C., Blavier, J. F. L., Boone, C., Bowman, K. P., Browell, E. V., Campos, T., Connor, B. J., Daube, B. C., Deutscher, N. M., Diao, M., Elkins, J. W., Gerbig, C., Gottlieb, E., Griffith, D. W. T., Hurst, D. F., Jiménez, R., Keppel-Aleks, G., Kort, E. A., Macatangay, R., Machida, T., Matsueda, H., Moore, F., Morino, I., Park, S., Robinson, J., Roehl, C. M., Sawa, Y., Sherlock, V., Sweeney, C., Tanaka, T., and Zondlo, M. A.: Calibration of the Total

Carbon Column Observing Network using aircraft profile data, Atmos. Meas. Tech., 3, 1351-1362, 10.5194/amt-3-1351-2010, 2010.

Wunch, D., Wennberg, P. O., Toon, G. C., Connor, B. J., Fisher, B., Osterman, G. B., Frankenberg, C., Mandrake, L., O'Dell, C., Ahonen, P., Biraud, S. C., Castano, R., Cressie, N., Crisp, D., Deutscher, N. M., Eldering, A., Fisher, M. L., Griffith, D. W. T., Gunson, M., Heikkinen, P., Keppel-Aleks, G., Kyrö, E., Lindenmaier, R., Macatangay, R., Mendonca, J., Messerschmidt, J., Miller, C. E., Morino, I., Notholt, J., Oyafuso, F. A., Rettinger, M., Robinson, J., Roehl, C. M., Salawitch, R. J., Sherlock, V., Strong, K., Sussmann, R., Tanaka, T., Thompson, D. R., Uchino, O., Warneke, T., and Wofsy, S. C.: A method for evaluating bias in global measurements of CO_2 total columns from space, Atmos. Chem. Phys., 11, 12317-12337, 10.5194/acp-11-12317-2011, 2011.

Yokota, T., Yoshida, Y., Eguchi, N., Ota, Y., Tanaka, T., Watanabe, H., and Maksyutov, S.: Global concentrations of CO_2 and CH_4 retrieved from GOSAT: Frst preliminary results, SOLA, 5, 160-163, 10.2151/sola.2009-041, 2009.

Yoshida, Y., Kikuchi, N., Morino, I., Uchino, O., Oshchepkov, S., Bril, A., Saeki, T., Schutgens, N., Toon, G. C., Wunch, D., Roehl, C. M., Wennberg, P. O., Griffith, D. W. T., Deutscher, N. M., Warneke, T., Notholt, J., Robinson, J., Sherlock, V., Connor, B., Rettinger, M., Sussmann, R., Ahonen, P., Heikkinen, P., Kyrö, E., Mendonca, J., Strong, K., Hase, F., Dohe, S., and Yokota, T.: Improvement of the retrieval algorithm for GOSAT SWIR XCO_2 and XCH_4 and their validation using TCCON data, Atmos. Meas. Tech., 6, 1533-1547, 10.5194/amt-6-1533-2013, 2013.

Figure Captions

Figure 1. Two regions considered in this study: Northeastern China-Korea (115˚E - 130˚E, 30˚N - 40˚N, gray-shaded) and Japan (130˚E - 145˚E, 30˚N - 40˚N, blue-shaded). The locations of the Saga and Tsukuba TCCON stations are marked by closed circles. The open circles are indicated the locations of the surface monitoring stations around Japan, Cape Ochi-ishi (COI), Ryori (RYO), and Yonagunijima (YON).

Figure 2. Temporal variations of GOSAT XCH_4 over the two regions of Northeast Asia: (a) Northeastern China – Korea (115˚E - 130˚E, 30˚N - 40˚N), and (b) Japan (130˚E - 145˚E, 30˚N - 40˚N). GOSAT XCH_4 data are shown in grey dot. The monthly means are plotted in red solid circle and line, whereas monthly means in open circles indicate less than two retrievals available per month. Blue lines indicate the long-term trends. The histogram in the bottom show the number of GOSAT XCH_4 data per month.

Figure 3. Locations of GOSAT soundings with the surface elevations, in the two regions considered in this study. The locations of three capital cities, Tokyo, Seoul and Beijing are also shown in black markers. (a) All soundings of GOSAT data used for 2009-2014. (b) Same with (a) but in August and September 2012. (c) Same with (a) but in August and September 2013.

Figure 4. Temporal variations of TCCON XCH4 at (a) Saga (130.29˚E, 33.24˚N) and (b) Tsukuba (140.12˚E, 36.05˚N), Japan. TCCON XCH_4 data are shown in grey dot, daily means in green dots. The monthly means are plotted in red solid circle and line, whereas monthly means in open circles indicate less than two observation days per month. Blue lines indicate the long-term trends. The histograms at the bottom show the number of observation day per month.

Figure 5. (a) Detrended XCH_4 for 2012 to 2013 at Saga and Tsukuba, Japan and GOSAT over Japan. (b) Same with (a) but also minus mean seasonal cycles. The

monthly means of the individual XCH_4 time series are shown in solid lines and circles. The open circles for TCCON indicate that observation days in a month are less than two days. The discontinuity of GOSAT in July 2012 indicates no GOSAT XCH_4 retrieval. Long-term components in individual XCH_4 time series are removed by low pass digital filter of cutoff frequency of two years. Mean seasonal cycles are composed of two harmonics of year and a half year cycles. August and September of both 2012 and 2013 are highlighted.

Figure 6. Temporal variations of atmospheric CH_4 concentrations observed at the ground-based monitoring sites around Japan, (a) Cape Ochi-ishi (COI, 43.16˚N, 145.49˚E), (b) Ryori (RYO, 39.03˚N, 141.82˚E), and (c) Yonagunijima (YON, 24.47˚N, 123.02˚E). The site locations are shown in Figure 1. Afternoon means of hourly CH_4 concentrations are shown in grey lines. The monthly means are plotted in red solid circle and line. Blue lines indicate the long-term trends.

Figure 7. Detrended CH4 for 2012 to 2013 at Ryori (RYO) and Cape Ochi-ishi (COI) in Japan. Long-term components in individual CH_4 time series are removed by low pass digital filter of cutoff frequency of two years. August and September of both 2012 and 2013 are highlighted.

Figure 8. Spatial distribution of monthly mean modelled (a) CH_4 and (b) XCH_4 in August and September of 2012 and 2013.

Figure 9. Model simulated XCH_4 time-series in comparison with the observed GOSAT XCH_4 over the two target regions of (a) Northeastern China-Korea and (b) Japan, and with the observed TCCON XCH_4 at (c) Saga and (d) Tsukuba. For GOSAT, modeled XCH_4 outputs are sampled at corresponding model grids and averaged by region. August and September of both 2012 and 2013 are highlighted.

Figure 10. Model simulated CH_4 time-series in comparison with the observed CH_4 at (a) Cape Ochi-ishi (COI, 43.16˚N, 145.49˚E), (b) Ryori (RYO, 39.03˚N, 141.82˚E),

and (c) Yonagunijima (YON, 24.47˚N, 123.02˚E). August and September of both 2012 and 2013 are highlighted.

Figure 11. Monthly mean wind fields of August and September at (a) surface and (b) 850hPa. The left panels are the wind fields averaged over the five years of 2009-2013, and the right panels are the monthly mean wind fields of the year 2013.

Figure 12. Monthly mean ten-day backward trajectories from (a) Saga and (b) Tsukuba at 12:00 noon local time (= 3:00 UT). The trajectories started at an altitude of 1500 m (approximately 850 hPa). 100 particles are released every day for a month. To normalize the number density of particles, the particles passed at each 1˚ x 1˚ grid air column are counted, and the total numbers are divided by the maximum number per grid.

Figure 1

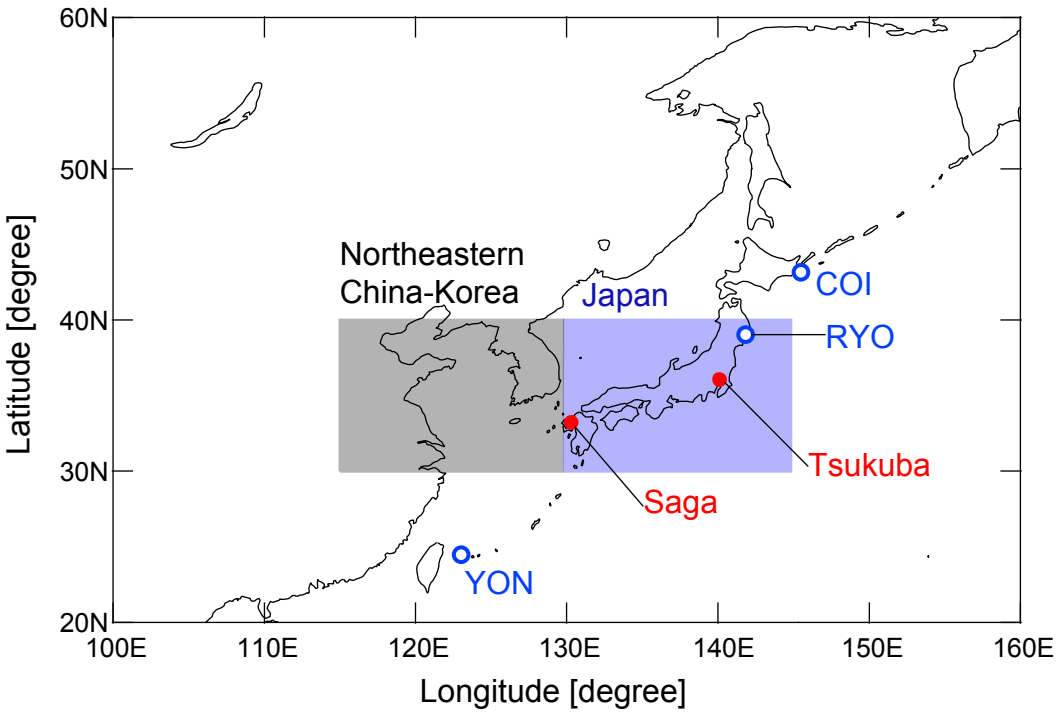

Figure 1. Two regions considered in this study: Northeastern China-Korea (115˚E -130˚E, 30˚N -40˚N, gray-shaded) and Japan (130˚E-145˚E, 30˚N-40˚N, blue-shaded). The locations of the Saga and Tsukuba TCCON stations are marked by closed circles. The open circles are indicated the locations of the surface monitoring stations around Japan, Cape Ochi-ishi (COI), Ryori (RYO), and Yonagunijima (YON).

Figure 2

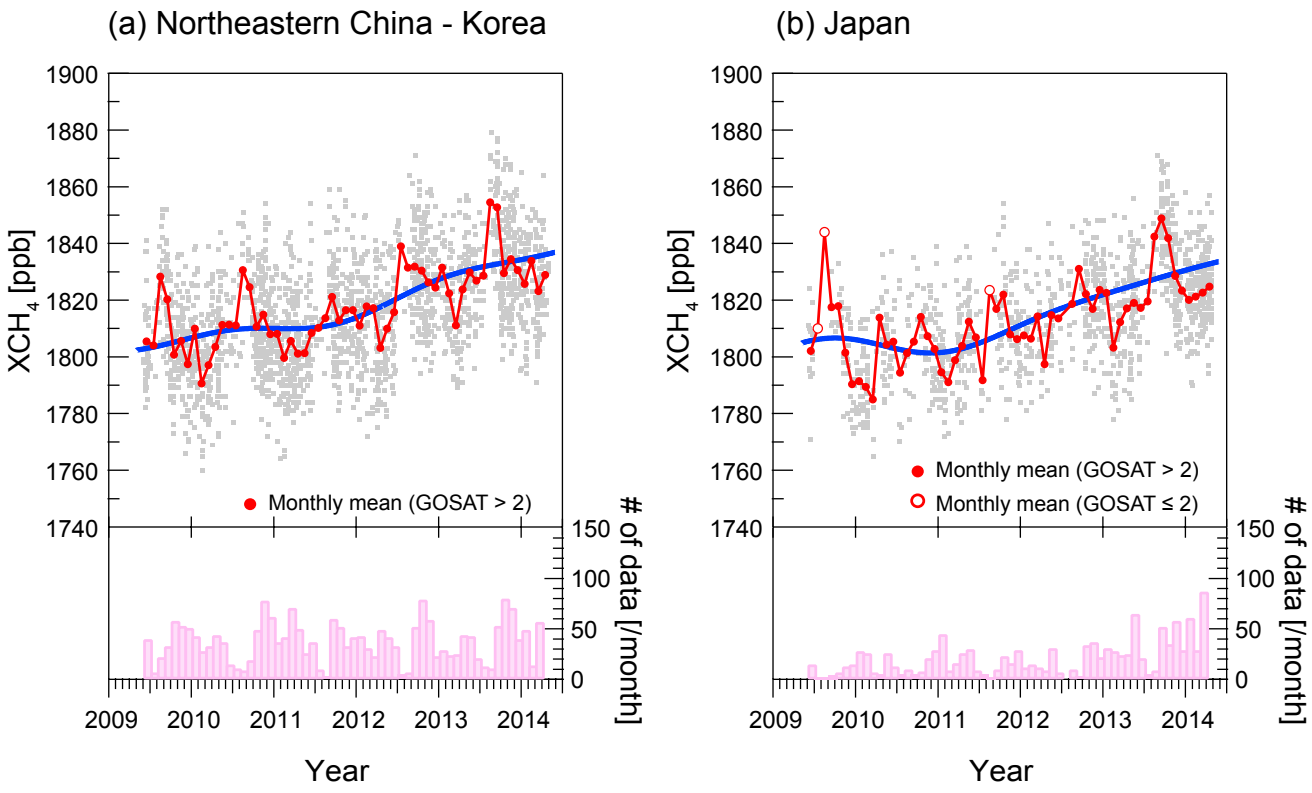

Figure 2. Temporal variations of GOSAT XCH_4 over the two regions of Northeast Asia: (a) Northeastern China – Korea (115˚E-130˚E, 30˚N-40˚N), and (b) Japan (130˚E-145˚E, 30˚N -40˚N). GOSAT XCH_4 data are shown in grey dot. The monthly means are plotted in red solid circle and line, whereas monthly means in open circles indicate less than two retrievals available per month. Blue lines indicate the long-term trends. The histogram in the bottom show the number of GOSAT XCH_4 data per month.

Figure 3

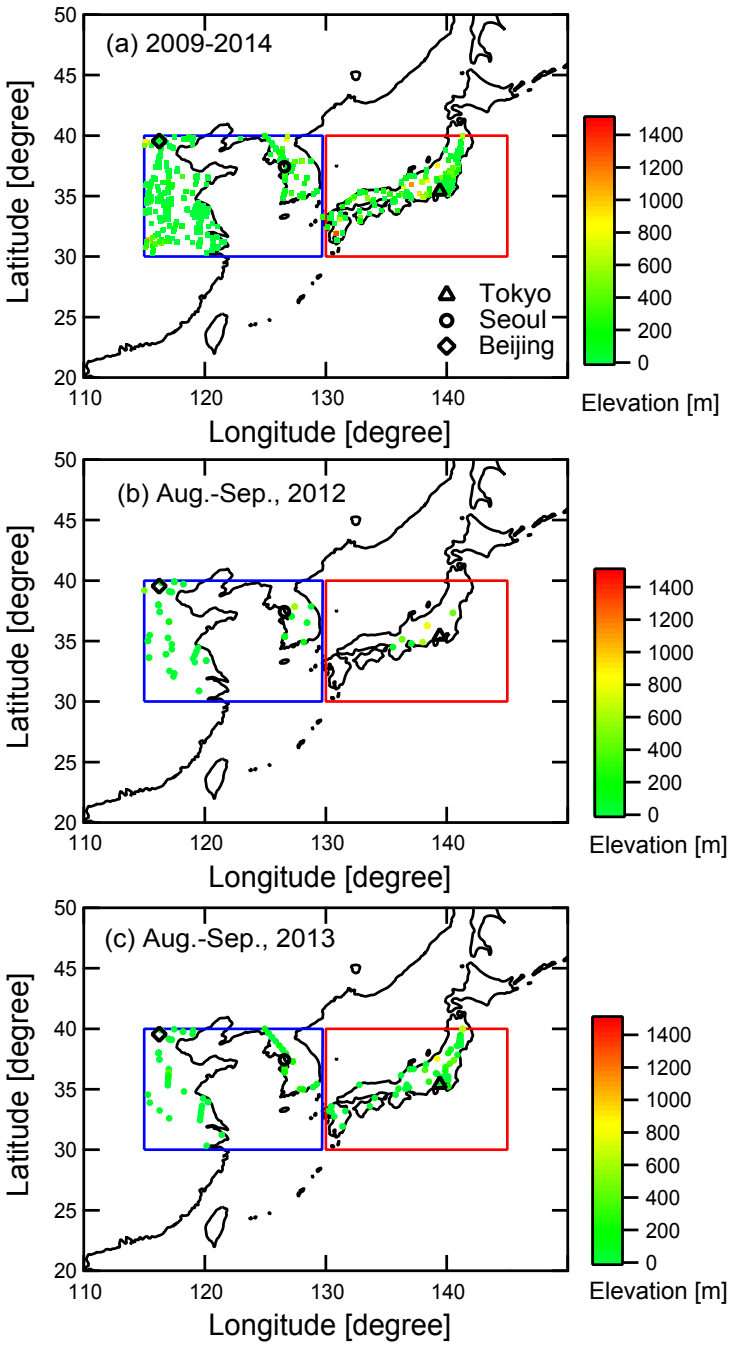

Figure 3. Locations of GOSAT soundings with the surface elevations, in the two regions considered in this study. The locations of three capital cities, Tokyo, Seoul and Beijing are also shown in black markers. (a) All soundings of GOSAT data used for 2009-2014. (b) Same with (a) but in August and September 2012. (c) Same with (a) but in August and September 2013.

Figure 4

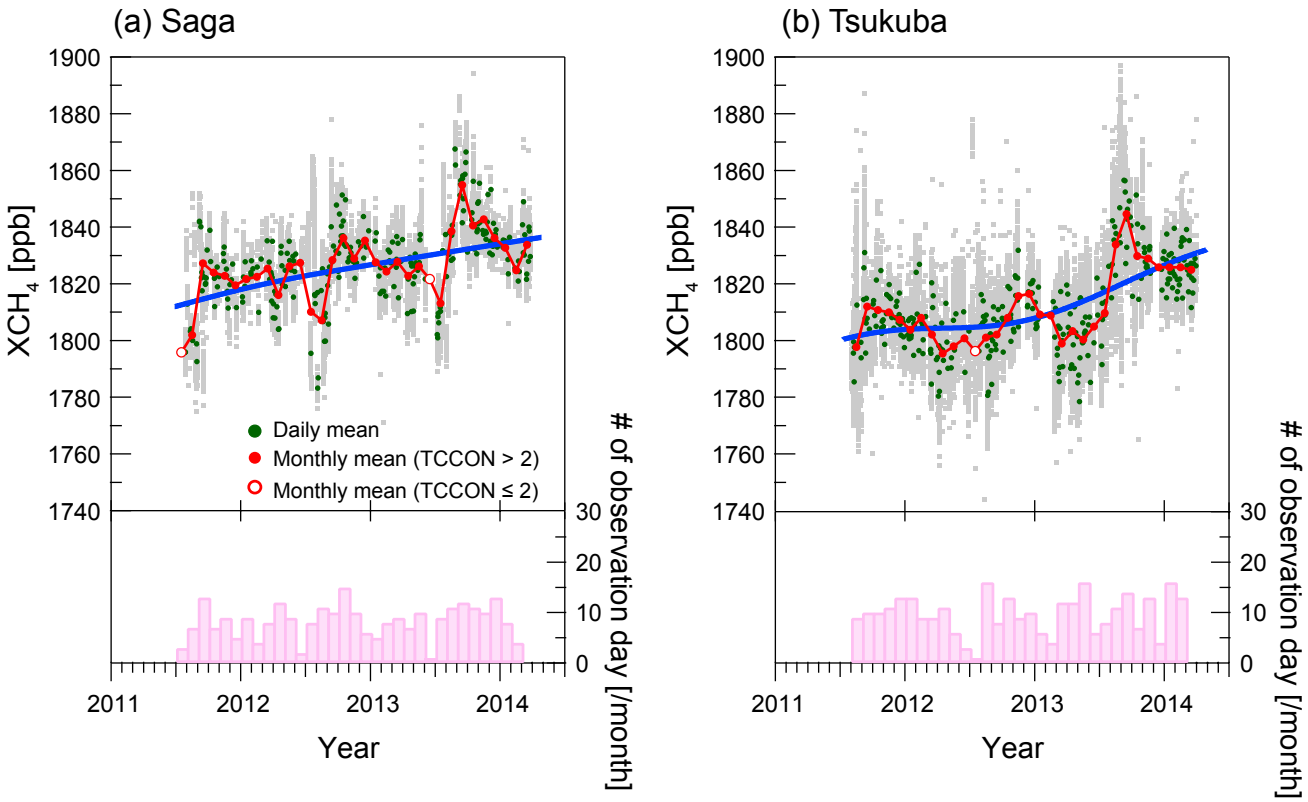

Figure 4. Temporal variations of TCCON XCH_4 at (a) Saga (130.29˚E, 33.24˚N) and (b) Tsukuba (140.12˚E, 36.05˚N), Japan. TCCON XCH_4 data are shown in grey dot, daily means in green dots. The monthly means are plotted in red solid circle and line, whereas monthly means in open circles indicate less than two observation days per month. Blue lines indicate the long-term trends. The histograms at the bottom show the number of observation day per month.

Figure 5.

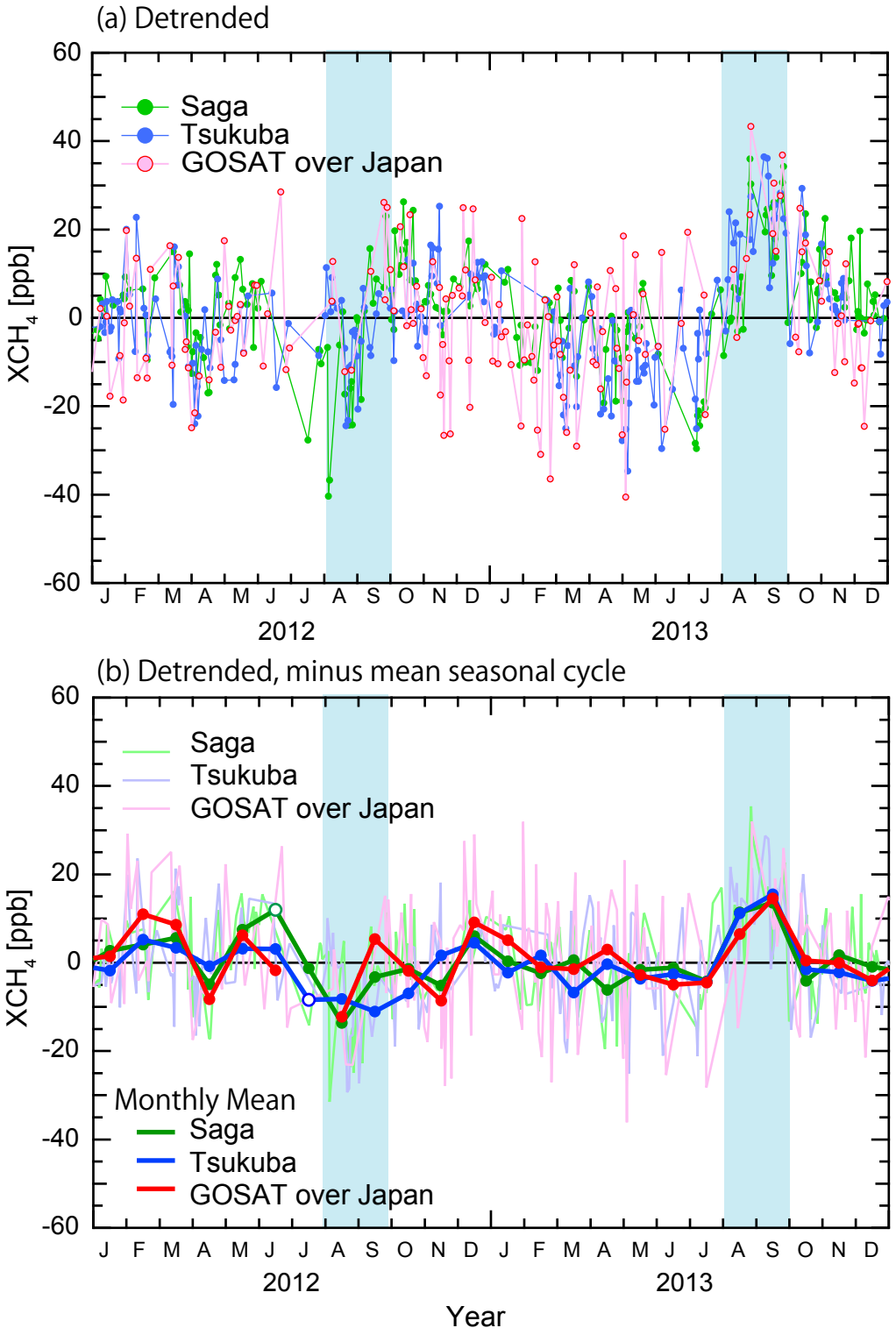

Figure 5. (a) Detrended XCH_4 for 2012 to 2013 at Saga and Tsukuba, Japan and GOSAT over Japan. (b) Same with (a) but also minus mean seasonal cycles. The monthly means of the individual XCH_4 time series are shown in solid lines and circles. The open circles for TCCON indicate that observation days in a month are less than two days. The discontinuity of GOSAT in July 2012 indicates no GOSAT XCH_4 retrieval. Long-term components in individual XCH_4 time series are removed by low pass digital filter of cutoff frequency of two years. Mean seasonal cycles are composed of two harmonics of year and a half year cycles. August and September of both 2012 and 2013 are highlighted.

Figure 6

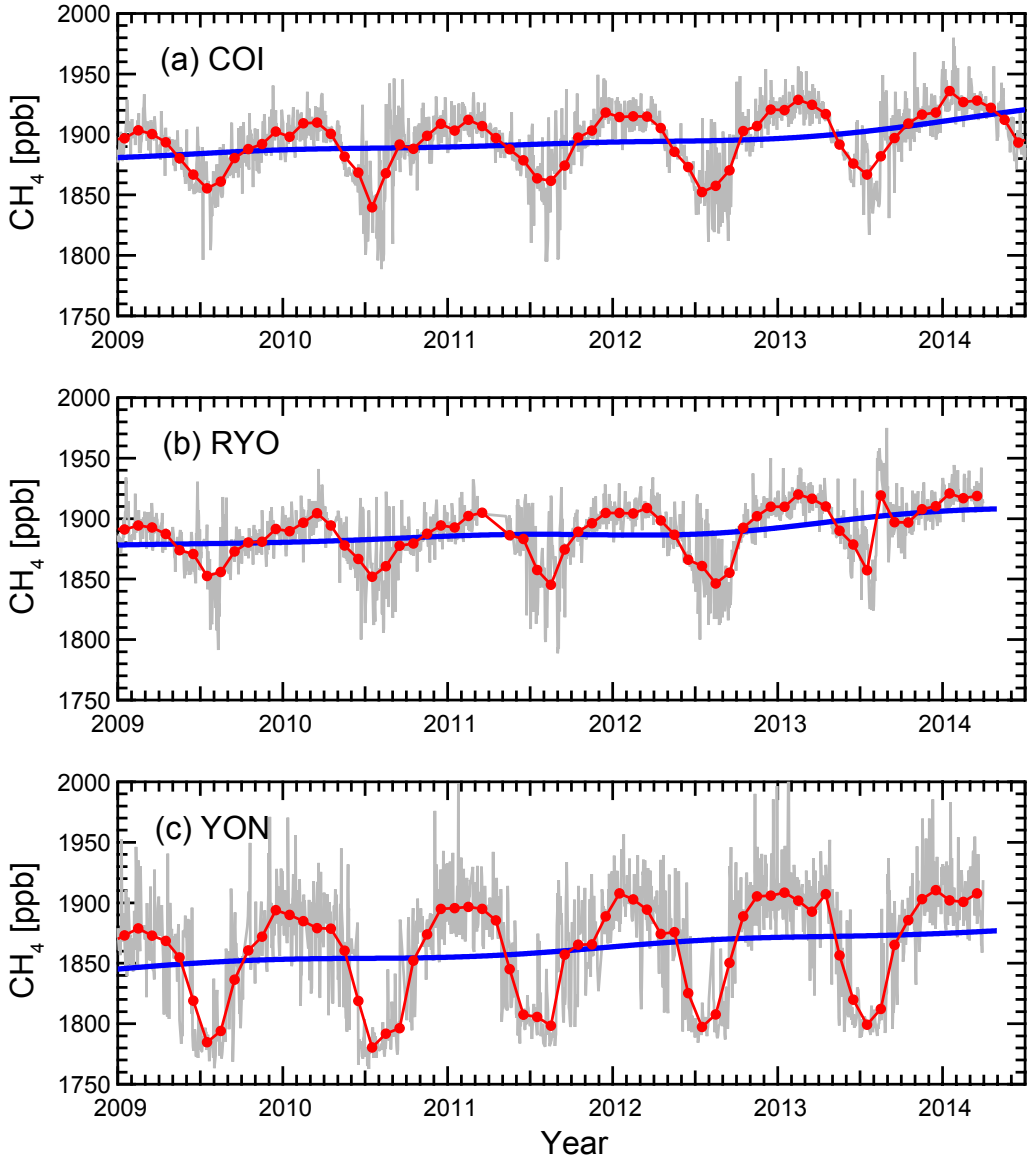

Figure 6. Temporal variations of atmospheric CH_4 concentrations observed at the ground-based monitoring sites around Japan, (a) Cape Ochi-ishi (COI, 43.16˚N, 145.49˚E), (b) Ryori (RYO (39.03˚N, 141.82˚E), and (c) Yonagunijima (YON, 24.47˚N, 123.02˚E). The site locations are shown in Figure 1. Afternoon means of hourly CH_4 concentrations are shown in grey lines. The monthly means are plotted in red solid circle and line. Blue lines indicate the long-term trends.

Figure 7

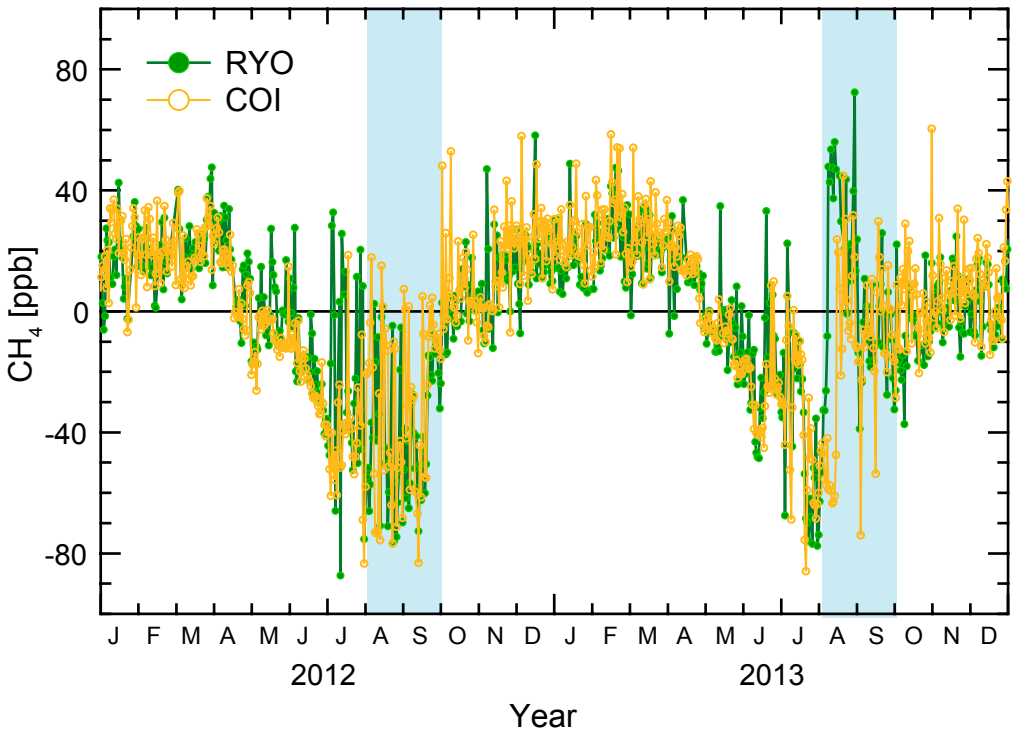

Figure 7. Detrended CH_4 for 2012 to 2013 at Ryori (RYO) and Cape Ochi-ishi (COI) in Japan. Long-term components in individual CH_4 time series are removed by low pass digital filter of cutoff frequency of two years. August and September of both 2012 and 2013 are highlighted.

Figure 8

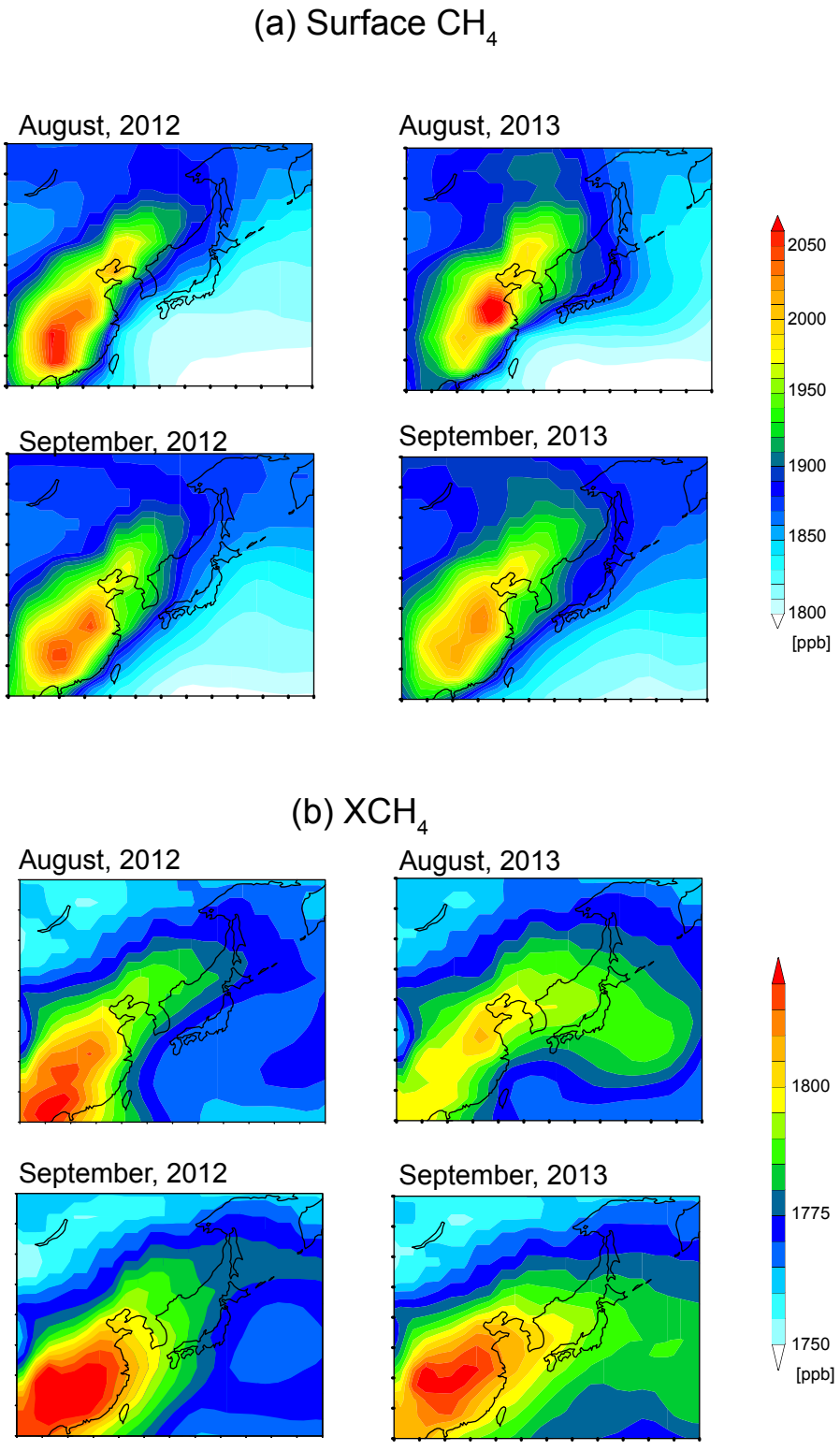

Figure 8. Spatial distribution of monthly mean modelled (a) CH_4 and (b) XCH_4 in August and September of 2012 and 2013.

Figure 9.

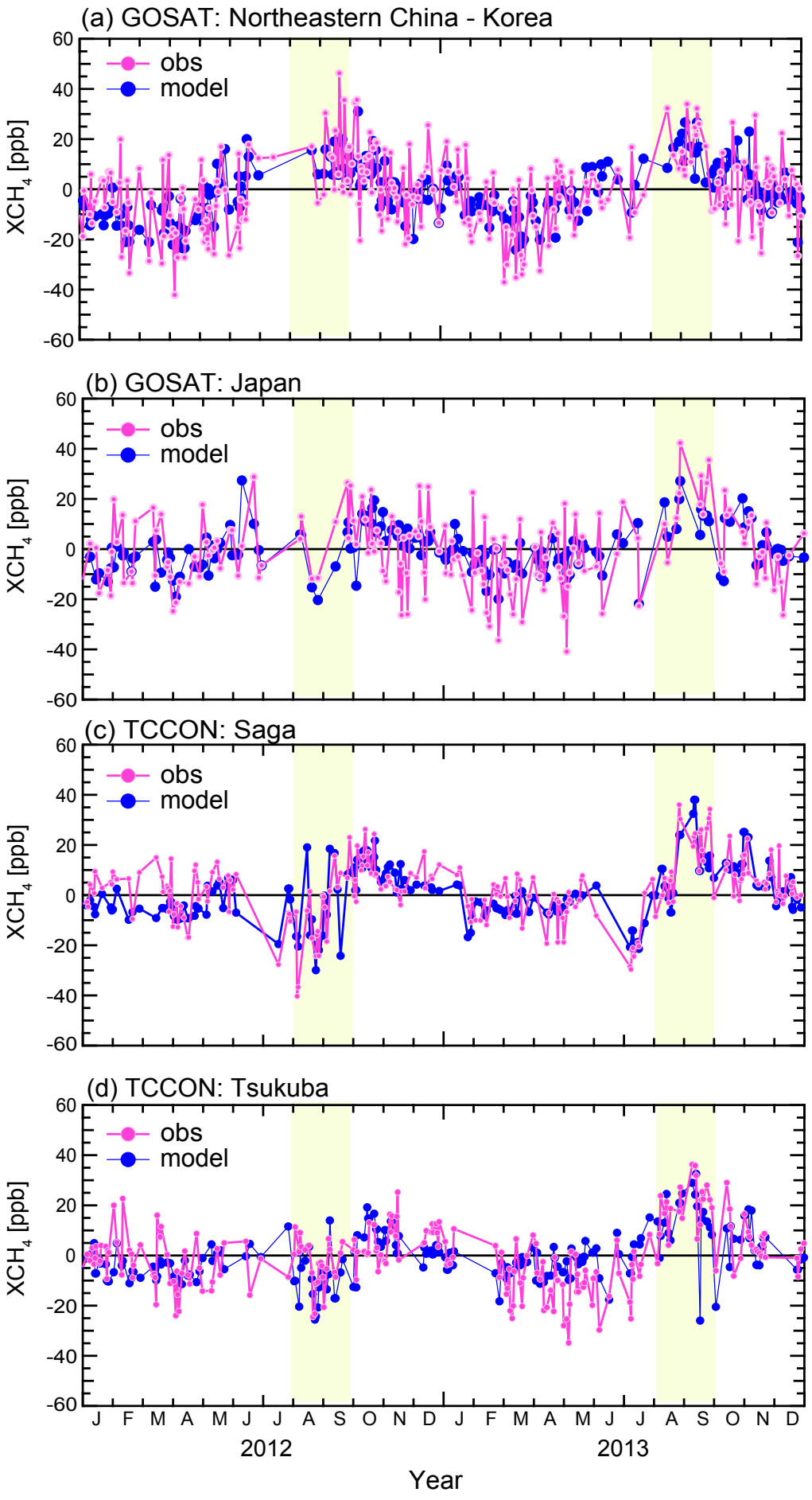

Figure 9. Model simulated XCH_4 time-series in comparison with the observed GOSAT XCH_4 over the two target regions of (a) Northeastern China-Korea and (b) Japan, and with the observed TCCON XCH_4 at (c) Saga and (d) Tsukuba. For GOSAT, modeled XCH_4 outputs are sampled at corresponding model grids and averaged by region. August and September of both 2012 and 2013 are highlighted.

Figure 10

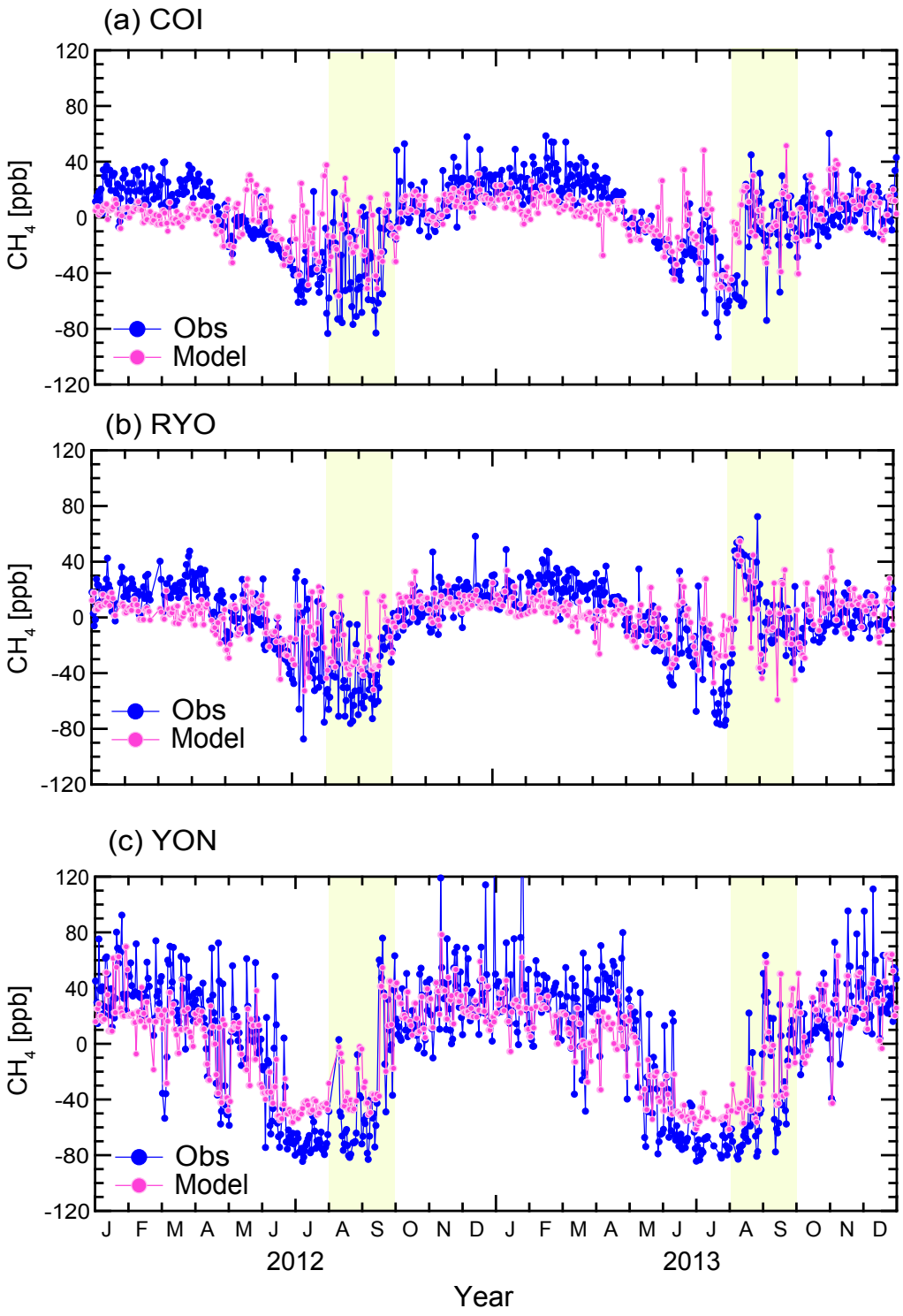

Figure 10. Model simulated CH_4 time-series in comparison with the observed CH_4 at (a) Cape Ochi-ishi (COI, 43.16˚N, 145.49˚E), (b) Ryori (RYO (39.03˚N, 141.82˚E), and (c) Yonagunijima (YON, 24.47˚N, 123.02˚E). August and September of both 2012 and 2013 are highlighted.

Figure 11

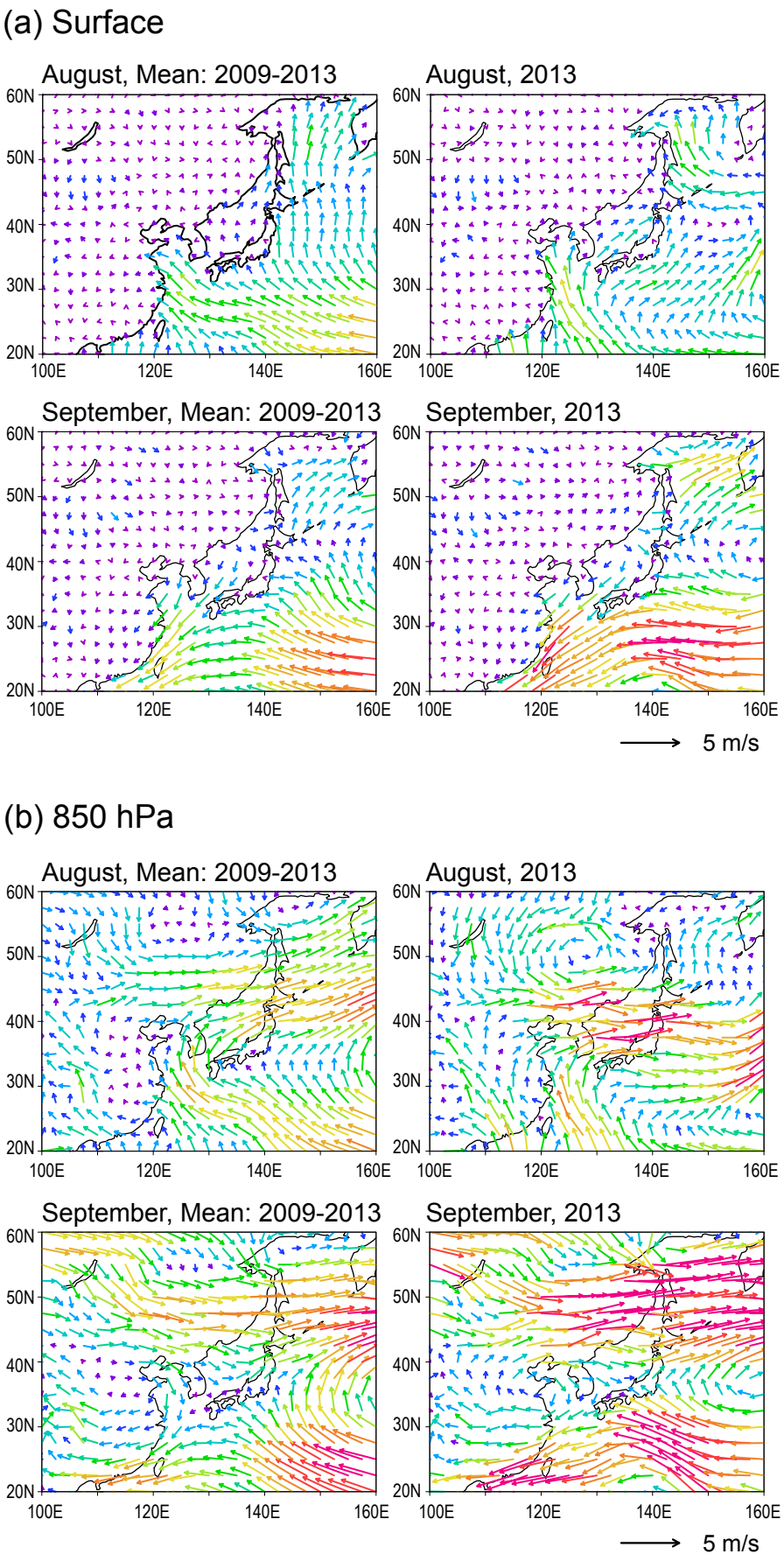

Figure 11. Monthly mean wind fields of August and September at (a) surface and (b) 850hPa. The left panels are the wind fields averaged over the five years of 2009-2013, and the right panels are the monthly mean wind fields of the year 2013.

Figure 12.

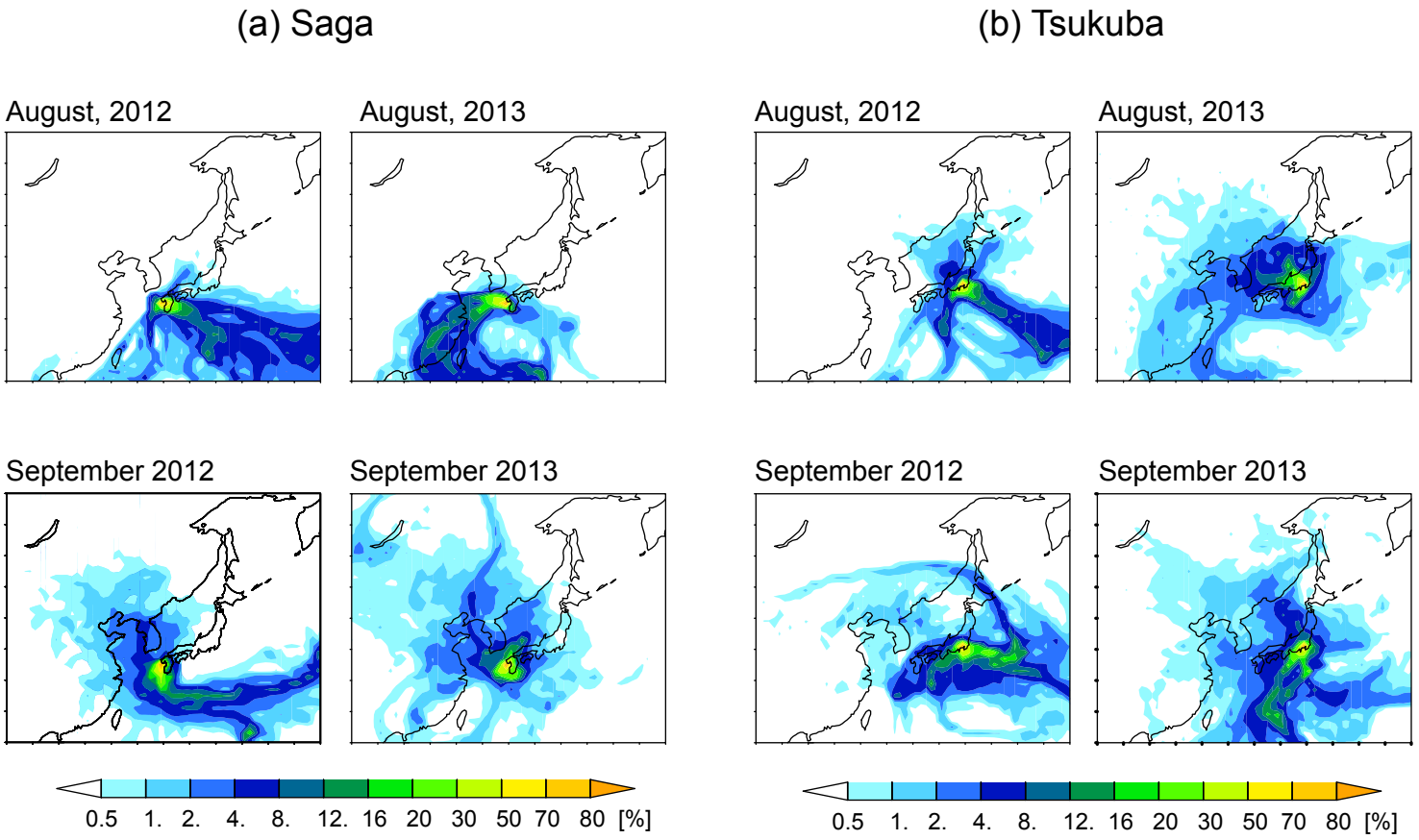

Figure 12. Monthly mean ten-day backward trajectories from (a) Saga and (b) Tsukuba at 12:00 noon local time (= 3:00 UT). The trajectories started at an altitude of 1500 m (approximately 850 hPa). 100 particles are released every day for a month. To normalize the number density of particles, the particles passed at each 1˚x1˚ grid air column are counted, and the total numbers are divided by the maximum number per grid.